Active mechanosensitivity of hair cells from the inner ear and of assemblies of molecular motors in vitro

Pascal Martin

HABILITATION A DIRIGER DES RECHERCHES

Université Pierre et Marie Curie – Paris 6

Spécialité :
Sciences Physiques

Mécanosensibilité active des cellules ciliées de l'oreille interne et d'une assemblée de moteurs moléculaires in vitro.

par Pascal Martin

Soutenue le 17 décembre 2010 devant le jury composé de :

M. Didier Chatenay	Rapporteur
M. Thomas Duke	Rapporteur
M. Vincent Hakim	
M. Jonathon Howard	Rapporteur
M. Frank Jülicher	
M. Jacques Prost	

TABLE OF CONTENTS

A. CURRICULUM VITAE : 4

B. RESEARCH 11

GENERAL OVERVIEW 11

I. INTRODUCTION 16
1. Psychophysical properties of hearing 16
2. The cochlear amplifier: 17
3. Mechano-electrical transduction by hair cells 20
   3.1 The hair bundle: a mechanical antenna 20
   3.2 The motor model of adaptation 22
   3.3 Calcium feedback 24
4. Methods to probe hair-bundle mechanics 26

II. ACTIVE HAIR-BUNDLE MOTILITY 27
1. Spontaneous hair-bundle oscillations 28
   1.1 Oscillation properties 28
   1.2 Negative stiffness 30
2. "Excitable" hair bundles – Mechanical correlates of adaptation 33
3. Calcium control of active hair-bundle motility 34
4. Physical description of active hair bundle motility 36
   4.1 Twitch 38
   4.2 Spontaneous oscillation 40
5. Using modeling to decipher the functional role of a protein expressed by a "deafness gene" in the transduction machinery 41

III. THE HAIR-BUNDLE AMPLIFIER 41
1. Mechanical amplification 41
   1.1 Power gain 41
   1.2 Compressive nonlinearity – Gain of the hair-bundle amplifier 44
2. Two-tone distortions and suppression by the hair-bundle amplifier 45
3. A useful concept: critical oscillation at a Hopf bifurcation 47
4. Intrinsic fluctuations and amplification by active hair-bundle oscillation 50
   4.1 Stochastic simulations of active hair-bundle motility 51
   4.2 Spontaneous movements and linear response of noisy oscillators: a general theoretical study 53
   4.3 Boosting the hair-bundle amplifier by mechanical coupling to "cyber clones" 54

IV. ACTIVE MOTILITY OF A MINIMAL ACTO-MYOSIN SYSTEM IN VITRO 56
1. Collective motor oscillations 57
2. Dynamical responsiveness of a motor collection to mechanical stimuli 59

C. FUTURE DIRECTIONS 63

I. Active hair-bundle motility by mammalian hair cells 63

II. Fluctuation-Response relation with an oscillatory hair-cell bundle 64

III. Dynamic mechanical properties of molecular-motor assemblies 65

REFERENCES: **69**

A. CURRICULUM VITAE :

PASCAL MARTIN

Laboratoire Physico-Chimie Curie, UMR168 CNRS, Institut Curie, UPMC
26, rue d'Ulm, 75248 Paris cedex 05

Tél. : + 33 (0)1 56 24 67 48
Fax : +33 (0)1 40 51 06 36
Email : Pascal.Martin@curie.fr

Né le : 21/10/1968
Nationalité : française

Cursus universitaire

Diplôme d'Université « Formation Spéciale à l'Expérimentation Animale », Avril 2002, suivi de l'autorisation d'expérimenter sur animaux vertébrés, Novembre 2002 et du certificat de capacité pour l'élevage de la grenouille taureau, Université Paris Descartes, Juin 2003.

Doctorat de l'Université Paris VI, Sciences Physiques, Juin 1997.

D.E.A de "Matière condensée : Chimie et Organisation", Université Paris VI, Juin 1993.

Diplôme d'Ingénieur de l'Ecole Supérieure de Physique et Chimie de la ville de Paris (E.S.P.C.I ; option : Physique), Juin 1993.

Parcours scientifique

Depuis Novembre 2006 : dirige, au sein de l'UMR168, l'équipe de l'Institut Curie, « Mecanosensibilité active des cellules ciliées de l'oreille interne »
Page web: http://www.curie.fr/recherche/transfert/savoir-faire.cfm/personnel/323/lang/_fr.htm

Octobre 2004 : Promotion au grade de CR1 du CNRS.

2001 2004 : dirige une jeune équipe ATIPE du CNRS.

Juillet 2000 : Admis au concours CNRS, section 11 (anciennement 15), niveau CR2, affectation à l'UMR168, Paris.

oct. 1997 – sept. 2000 : Post-doctorant, Howard Hughes Medical Institute at the Rockefeller University, Laboratory of Sensory Neuroscience, New York, Etats Unis.
Responsable : Dr. A. J. [Jim] Hudspeth
Sujet : « Amplification de stimuli mécaniques par les cellules ciliées de l'oreille interne des vertébrés »

nov.1994 - oct.1997 : Thèse, équipe «Surfaces douces» de l'UMR168, Institut Curie, en collaboration avec Michelin (bourse C.I.F.R.E).
Responsable : Prof. Françoise Brochard-Wyart

Sujet : « Démouillage d'un film liquide intercalé entre un solide et un milieu déformable »

jan.1992-nov.1994 : Stage de D.E.A, équipe «Surfaces douces» de l'UMR168, Institut Curie.
Responsable : Prof. Françoise Brochard-Wyart
Sujet : « Démouillage d'un film liquide déposé sur un substrat liquide »

Contrats de recherche

nov. 2001 – nov. 2004 : Action Thématique Incitative sur Programme et Equipe (ATIPE « Neurobiologie : du moléculaire au cognitif ») du département des Sciences de la Vie du CNRS pour la création d'une équipe.

nov. 2002 – oct. 2005 : Action Concertée Incitative (ACI) du ministère chargé de la recherche « Interface Physique-Chimie-Biologie : Dynamique et Réactivité des Assemblages Biologiques ». Collaboration avec les groupes dirigés par Jacques Prost (porteur du projet ; UMR168, Institut Curie) et Christine Petit (URA1968, Institut Pasteur).

2002 – 2004 : ACI du ministère chargé de la recherche « Interface Physique-Chimie-Biologie : Dynamique et Réactivité des Assemblages Biologiques ». Collaboration avec le groupe dirigé par Michel Bornens (porteur du projet ; UMR144, Institut Curie).

juin 2003 – nov 2006 : Subvention du Human Frontier Science Program (HSFP). Collaboration avec les groupes dirigés par Mats Ulfendahl (porteur du projet ; Karolinska Institute, Suède), Jacques Prost (UMR 168, Institut Curie), Hiroshi Wada (Tohoku University, Japan) et Charles Steele (Standford University, Etats Unis).

déc. 2004 – nov. 2009: équipe participante du European Union's Sixth Framework Programme (FP6). Integrated project: "*EuroHear*".

Production scientifique

Revues avec comité de lecture

1. Brochard-Wyart F, Martin P, Redon C (1993) Liquid/Liquid Dewetting. Langmuir 9: 3682-3690.
2. Martin P, Buguin A, Brochard-Wyart F (1994) Bursting of a liquid film on a liquid substrate. Europhys Lett 28:421-426.
3. Debrégeas G, Martin P, Brochard-Wyart F (1995) Viscous Bursting of Suspended Films. Phys Rev Let 75:3886.
4. Brochard-Wyart F, Debrégeas G, Fondecave R, Martin P (1996) Bursting of supported viscoelastic polymer rims: birth of rims. Macromolecules 30: 1211-1213.
5. Martin P, Silberzan P, Brochard-Wyart F (1997) Sessile Droplets at a Solid/Elastomer Interface. Langmuir 13:4910-4914.
6. Martin P, Brochard-Wyart F (1998) Dewetting at Soft Interfaces. Phys Rev Let 80: 3296
7. Martin P, Hudspeth AJ (1999) Active hair-bundle movements can amplify a hair cell's response to oscillatory mechanical stimuli. Proc Natl Acad Sci USA 96:14306-14311.

8. Brochard-Wyart F, Buguin A, Martin P, Martin A, Sandre O (2000) Adhesion of soft objects on wet substrates. J. Phys.: Condens. Matter 12:A239.

9. Martin P, Mehta AD, Hudspeth AJ (2000) Negative hair-bundle stiffness betrays a mechanism for mechanical amplification by the hair cell. Proc Natl Acad Sci USA 97:12026-12031.

10. Hudspeth AJ, Choe Y, Mehta AD, Martin P (2000) Putting ion channels to work: Mechanoelectrical transduction, adaptation, and amplification by hair cells. Proc Natl Acad Sci USA 97:11765-11772.

11. Martin P, Hudspeth AJ, Jülicher F (2001) Comparison of a hair bundle's spontaneous oscillations with its response to mechanical stimulation reveals the underlying active process. Proc Natl Acad Sci USA 98:14380-14385.

12. Martin P, Hudspeth AJ (2001) Compressive nonlinearity in the hair bundle's active response to mechanical stimulation. Proc Natl Acad Sci USA 98:14386-14391.

13. Martin P, Bozovic D, Choe Y, Hudspeth AJ (2003) Spontaneous oscillation by hair bundles of the bullfrog's sacculus. J Neurosci 23(11):4533-48.

14. Nadrowski B, Martin P, Julicher F (2004) Active hair-bundle motility harnesses noise to operate near an optimum of mechanosensitivity. Proc Natl Acad Sci USA 101(33):12195-12200.

15. Tinevez J-Y, Jülicher F, Martin P (2007) Unifying the various incarnations of active hair-bundle motility by the vertebrate hair cell. Biophys J 93:4053-4067

16. Michalski N, Michel V, Bahloul A, Lefevre G, Barral J, Yagi H, Chardenoux S, Weil D, Martin P, Hardelin JP, Sato M, Petit C (2007) Molecular characterization of the ankle-link complex in cochlear hair cells and its role in the hair bundle functioning. J Neurosci 27:6478-6488

17. Clausznitzer D, Lindner B, Jülicher F, Martin P (2008) Two-state approach to stochastic hair bundle dynamics. Phys Rev E 77:041901

18. Michalski N, Michel V, Lefèvre G, Caberlotto E, Tinevez J-Y, Bezard E, Weil D, Hardelin J-P, Martin P, Petit C (2009) Harmonin-b, an actin-binding scaffold protein, is involved in the adaptation of mechanoelectrical transduction by sensory hair cells. Pflugers Arch 459:115-130

19. Jülicher F, Dierkes K, Lindner B, Prost J, Martin P (2009) Spontaneous movements and linear response of a noisy oscillator. Eur Phys J E 29:449-460

20. Plaçais PY, Balland M, Guérin T, Joanny J-F, Martin P (2009) Spontaneous oscillations of a minimal acto-myosin system under elastic loading. Phys Rev Lett 103:158102

21. Guérin T, Prost J, Martin P, Joanny JF (2010) Coordination and collective properties of molecular motors: theory. Curr Opin Cell Biol 22:14-20.

22. Barral J, Dierkes K, Lindner B, Jülicher F, Martin P (2010) Coupling a sensory hair-cell bundle to cyber clones enhances nonlinear amplification. Proc Natl Acad Sci USA 107:8079-8084.

23. Ashmore J, Avan P, Brownell WE, Dallos P, Dierkes K, Fettiplace R, Grosh K, Hackney CM, Hudspeth AJ, Jülicher F, Lindner B, Martin P, Meaud J, Petit C, Santos Sacchi JR, and Canlon B (2010) The remarkable cochlear amplifier. Hear Res. 266:1-17

24. Hudspeth AJ, Jülicher F, Martin P (2010) A critique of the critical cochlea: Hopf, a bifurcation, is better than none. J Neurophysiol 104: 1219-1229

Proceedings avec comité de lecture

1. Brochard-Wyart F, Martin P (1996) Adhesion of a soft rubber on a wet solid. Journal of Adhesion 67:139-151. Symposium on Fundamentals of Adhesion and Interfaces at the Fall Meeting of the American-Chemical-Society, AUG 25-28, 1996 Orlando, Florida, USA.

2. Brochard-Wyart F, Buguin A, Martin P, Martin A, Sandre O (1999) Adhesion of soft objects on wet substrates. J. Phys. : Condens. Matter 12:A239-A244. 4th Liquid Matter Conference, JUL 03-07, 1999, Granada, Spain ,.

3. Martin P, Jülicher F, Hudspeth AJ (2002). The contribution of transduction channels and adaptation motors to the hair cell's active process. Biophysics of the Cochlea: From Molecules to Models. Proceedings of the International Symposium held in Titisee, Germany, JUL 27-AUG 1, 2002, pp 3-15

4. Nadrowski B, Martin P, Julicher F (2005) Spontaneous oscillations in mechanosensory hair bundles. Fluctuations and Noise in Biological, Biophysical, and Biomedical Systems III Book Series: Proceedings of the Society of Photo-Optical Instrumentaion Engineers (SPIE) 5841: 17-22. Conference on Fluctuations and Noise in Biological, Biophysical, and Biomedical Systems III, MAY 24-26, 2005 Austin, TX, USA.

5. Martin P, Nadrowski B, Jülicher F (2005). Active hair-bundle motility harnesses noise to operate near an optimum of mechanosensitivity, Auditory Mechanisms: Processes and Models: Proceedings of the Ninth International Symposium held in Portland, Oregon, USA, JUL 23-28, 2005, pp474-481

6. Martin P, Tinevez J-Y, Jülicher F (2008) Active hair-bundle motility by the vertebrate hair cell, Proceedings of the 10th International Workshop on the Mechanics of Hearing jeld in Keele, UK, JUL 27-31, 2008

7. Martin P, Barral J, Dierkes K, Lindner B, Jülicher F (2010) The hair cell as a sensory receptor and amplifier for hearing, US National Congress on Theoretical and Applied Mechanics, University of Pennsylvania, USA, JUN 27-JUL 2, 2010

Chapitre d'ouvrage

Martin P (2008) Active hair-bundle motility of the hair cells of vestibular and auditory organs. In: Active processes and otoacoustic emissions (Manley GA, Popper AN, Fay RR, eds), pp 93-144. New York: Springer

Conférences invitées

1. Symposium "Biophysics of the cochlea : from molecules to models", Titisee, Allemagne, Juillet 2002 .

2. Colloque "Invasion Phenomena in Biology and Ecology", Institut Henry Poincaré, Paris, Novembre 2002.

3. Colloque “Motion, sensation and self−organization in living cells”, MPIPKS, Dresde, Allemagne, Octobre 2003.
4. Colloque “Molecular motors”, Bad Honnef, Allemagne, Avril 2004.
5. Colloque “Complex dynamical processes in electroreceptors and hair cells”, MPIPKS, Dresde, Allemagne, Mai 2004.
6. Journée de la matière condensée de la Société Française de Physique, Nancy, Août 2004.
7. Colloque “Sensory Processing, Learning and Cognition – theoretical and experimental approaches”, Fondation Les Treilles, Tourtour, France, Septembre 2004.
8. Colloque “Controlled Nanoscale Motion in Artificial and Biological Systems”, Bäckaskog Castle, Suède, Juin 2005.
9. Séminaire Dautreppe « Physique du vivant : molécules, assemblages, signalisation, réseaux », Société Française de Physique, Grenoble, Septembre 2005.
10. Journée de la physique non linéaire, Institut Poincaré, Mars 2006.
11. Symposium “Perspectives in physics of biological and non linear systems”, Faculté de Physique de l’Université Georg August, Göttingen, Allemagne, Avril 2006.
12. Colloque “Dynamic Days 2006”, Heraklion, Grèce, Septembre 2006.
13. Symposium “Dynamic behaviour of the organ of Corti”, Aomori, Japon, Octobre 2006
14. Annual meeting of the German Society of Physics (DPG), Regensburg, Allemagne, Mars 2007.
15. Colloque “The structure and operation of the hair bundle”, Paris, France, Avril 2007.
16. Colloque “Franco-Israeli trends 2007”, Biarritz, France, Octobre 2007.
17. Ecole de Physique des Houches « Collective effects in Cell Biology », Avril 2008.
18. Conférence « Force-gated ion channels », Janelia Farm, Washington (USA), Mai 2008.
19. Gordon conference “Muscle and molecular motors”, Colby Sawyer College, New London (USA), Juillet 2008.
20. Conférence “Mechanics of hearing”, Keele (UK), Juillet 2008.
21. Symposium “The hair cell as a sensory receptor and amplifier for audition and balance” au sein de la conférence de l’International Union of Physiological Sciences (IUPS), Kyoto (Japon), Juillet 2009.
22. Conférence “De Gennes Days on Physics of Cellular Mechanosensing”, Isrotel Dead Sea (Israel), Janvier 2010.
23. Conférence “Mechanics of cells and tissues: sensing, generating and coordinating forces in biological systems”, Titisee (Allemagne), Mars 2010.
24. Workshop “The physics of hearing and neurons meets nanoelectromechanics”, Pohang (Corée du sud), Juillet 2010
25. Workshop “Structure formation and transport in complex systems”, Saarbrucken (Allemagne), Septembre 2010

26. Workshop "Physics and Neuroscience: heading towards quantitative biology", II Joint Meeting of the Argentine Society for Research on Neurosciences (SAN) and the Argentine Workshop in Neurosciences (TAN), Huerta grande (Argentine), Octobre 2010.

Séminaires

1. Université de Pharmacie de Chatenay Malabry, UMR8612 (2003)
2. Groupe Matière et Systèmes Complexe, Université Paris 7, Paris (2003)
3. Groupe de Physique des Solides, Université Paris 6-7, Campus Boussicault, Paris (2004)
4. Isaac Newton Institute for Mathematical Sciences, dans la série de seminaries "Statistical Mechanics of Molecular and Cellular Biological Systems", Cambridge, Royaume Uni (2004)
5. Ecole Normale Supérieure, dans la série des séminaires de biophysique, Paris (2004)
6. Laboratoire de Physiologie Cellulaire de la Synapse, UMR5091, Bordeaux (2004)
7. Collège de France (cours de Christine Petit), Paris (2004)
8. National Institute for Medical Research, Londre, Royaume Uni (2004)
9. Laboratory of Sensory Neuroscience, the Rockefeller University, New York, Etats-Unis (2004)
10. IUSTI, Marseilles (2004)
11. Laboratory of Sensory Neuroscience, the Rockefeller University, New York, Etats Unis (2005)
12. Department of Otolaryngology, Columbia University, New York, Etats Unis (2005)
13. Université de Physique de Padoue, Italie (2006)
14. Laboratoire de Physique des Solides, Ecole Polytechnique (2006)
15. Department of Biological Sciences, University of Bristol, Royaume Uni (2007)
16. Collège de France (cours de Christine Petit), Paris (2008)
17. Ecole Normale Supérieure (pour les étudiants du parcours Physique), Paris (2008)
18. Laboratoire MSC – UMR7057, Université Paris Diderot, Paris (2009)
19. Service de Physique de l'Etat Condensé (SPEC), Institut Rayonnement Matière Saclay (IRAMIS), Saclay (2009)
20. University College London, Ear Institute, Londres, Royaume Uni (2009)
21. Séminaire Rhône-Alpin de Modélisation du Vivant (SEMOVI), Lyon (2010)

Encadrement

1. Jean-Yves Tinevez – stagiaire de Master 2 puis doctorant d'Octobre 2002 à Mars 2006. Thèse de l'Université Paris Diderot (ED381) soutenue le 10 Mars 2006. Sujet : « Mouvements actifs, régulés par le calcium, de la touffe ciliaire mécanosensible des cellules ciliées de l'oreille

interne. » Financement : allocation couplée Université Paris Diderot - ENS Cachan. Actuellement en postdoc à l'Institut Pasteur.

2. Kirill Evlempiev – stagiaire de Master 2 (parcours Physique Théorique) de Mai à Juin 2004. Sujet : « Maintient dynamique de la structure en tuyaux d'orgue de la touffe ciliaire des cellules ciliées de l'oreille interne ». Après le stage, Kirill a effectué une thèse théorique dans le groupe dirigé par Hervé Isambert dans notre département.

3. Martial Balland –stage post doctoral de Décembre 2004 à Août 2006. Sujet : « Etude des propriétés mécaniques collectives de la myosine ». Actuellement Maître de Conférence à l'Université Joseph Fourier de Grenoble.

4. Pierre-Yves Plaçais – en thèse d'Octobre 2004 à Juin 2008. Thèse de l'Université Pierre et Maris Curie (ED107) soutenue le 6 juin 2008. Sujet : « Propriétés mécaniques de la myosine II in vitro : de la molécule unique aux effets collectifs ». Financement : allocation couplée UPMC – ENS Lyon. Actuellement post-doctorant dans le groupe de Thomas Préat à l'ESPCI, Paris.

5. Jérémie Barral – stagiaire de Master 2 de février à juin 2006 puis en thèse à partir d'Octobre 2006 (ED474 ; soutenance prévue en Septembre 2010). Sujet : « L'amplificateur ciliaire des cellules ciliées de l'oreille interne ». Financement : allocation couplée Université Paris Diderot – ENS Paris.

6. Jean Geoffroy – stagiaire de L3 (parcours Phytem de l'ENS Cachan), mois de Juin 2007. Sujet : « Test de motilité de villosités d'actine isolées sur un tapis de myosines in vitro ». Actuellement en thèse à l'ENS Paris.

7. Joseph Jackson – stage post doctoral (Février 2008- Février 2009). Sujet : « Propriétés mécaniques collectives de la myosine II ». Actuellement en postdoc à l' Université de Strathclyde, Glasgow (Royaume Uni).

8. Jonathan Lee-Tin-Wah – étudiant en thèse (ED474) depuis Octobre 2009. Sujet : « Assemblées de moteurs moléculaires sous contrainte élastique : oscillations spontanées et réponse dynamique aux stimuli externes ». Financement : Allocation fléchée sur Sujets Prioritaires.

Enseignement

2003 - 2004 : Cours « Mouillage, adhésion »
Institut de Sciences et Technologie (Paris), cours de 3ème année, 30 étudiants, 10 heures par an.

2007 - 2010 : Travaux dirigés de Physique en Médecine (PCEM1), UFR Biomédicale de l'Université Paris Descartes, deux groupes de 40 étudiants, 66 heures par an.

2007 - 2008 et *2009-2010* : Cours « Physique de l'audition », Ecole Doctorale de Physique de la Région Parisienne (ED107), 10 étudiants, 15 heures

2008 - 2010 : Cours « Physique de l'audition », Master 1 de Biologie de l'Ecole Normale Supérieure, 10 étudiants, 12 heures (Paris)

2008 – 2010 : Travaux dirigés (8 heures par an ; 24 élèves) et Tutorat (16 heures par an ; groupes de 4 élèves) de Physique Statistique en première année de l'ESPCI.

B. RESEARCH

GENERAL OVERVIEW

After completing undergraduate studies in Physics and Chemistry, I did my PhD between 1994 and 1997 under the supervision of Françoise Brochard in the Laboratoire Physico-Chimie Curie of the Institut Curie. My thesis dealt with the properties of thin liquid films (~100 nm) that were formed by squeezing a deformable rubber bead against a flat, rigid and hydrophobic substrate. This geometry is of practical interest, in particular in the case of the lachrymal film that is intercalated between the cornea and a contact lens or when driving on a wet road. The latter situation prompted a collaboration with the Michelin tyre-company that financed my thesis. In this work, I defined the conditions that controlled the stability of an intercalated film and, in the case where a dry contact between the two solids was energetically favourable, measured dewetting kinetics (Martin and Brochard-Wyart, 1998). The results were interpreted within the framework of a hydrodynamic description of intercalated dewetting that was introduced earlier by Françoise and the late Pierre-Gilles de Gennes. I won't give more details about my PhD work but would like to stress that I was positively impressed, as a young experimentalist, by the opportunity to work with an enthusiastic theorists (my thesis advisor) on an everyday basis. In my opinion, the tight interplay between theory and experiment remains a trademark of research performed at the Laboratoire Physico-Chimie Curie and makes this department of the Curie Institute particularly attractive. My thesis also happened at the time when Didier Chatenay and his colleagues were pulling on single DNA molecules, when the group lead by Albrecht Ott was looking for the first in-vitro evidence of dynamic transitions in collections of molecular motors, which that had just been predicted by Jacques Prost and Frank Jülicher. These and other projects at the interface between physics and biology felt like adventure and I thus naturally became interested in working on biological systems.

Following an advice given by Didier Chatenay, I did my postdoc under the supervision of Jim Hudspeth in the Laboratory of Sensory Neuroscience at the Rockefeller University (New York, USA). I was completely ignorant in biology. Being found of music of all kinds and immediately seduced by the scientific aura of Jim Hudspeth, I nevertheless found attractive to

work in a laboratory devoted to the vertebrate ear. I thus started studying the active mechanical properties of the ear's mechanoreceptor "hair cells", and soon realized that there was a lot of interesting physics involved. These highly specialized cells mediate transduction of sound-evoked mechanical vibrations into electrical signals that then propagate along nervous pathways to the brain. The main achievement of my postdoc was to demonstrate in vitro that a hair cell can power spontaneous oscillations of its mechanoreceptive organelle – the hair bundle – and harness these active movements to enhance the sensitivity, sharpen the frequency selectivity and widen the dynamical range of the sensory process (Martin and Hudspeth, 1999; Martin and Hudspeth, 2001; Martin et al., 2003). We also set the basis for the mechanism that would explain how spontaneous hair-bundle oscillations arise (Martin et al., 2000; Martin et al., 2003). In the model, active hair-bundle movements are powered by molecular motors of the myosin type and rely on electro-mechanical feedback by the calcium component of the transduction current. The properties of the hair-bundle amplifier were recognized by theorists, including Marcello Magnasco (from the Rockefeller University), Jacques Prost, Tom Duke and Frank Jülicher (then all working at the Curie Institute), as signatures of an active dynamical system operating near an oscillatory instability, the Hopf bifurcation. The generic nonlinear physics of so-called "critical oscillators" turned out to provide a useful theoretical framework to apprehend our experiments at the level of the single hair cell and, more generally, to offer a general description of the remarkable technical specifications of vertebrate hearing (Hudspeth et al., 2010).

After I got a CNRS position of "chargé de recherche" in the summer of 2000, I promptly returned to the Curie Institute to expand the work on active hair-cell mechanics that was initiated with Jim Hudspeth during my postdoc. Although I was originally a researcher in the group "Soft interfaces" of the Laboratoire Physico-Chimie Curie, Françoise Brochard, who headed this group, gave me complete freedom to develop my own line of research. In addition, in accordance with a requirement of the ATIPE grant of the CNRS that I had just received, Jacques Prost, who was then the head of the department, took the decision to allocate 50 m^2 of lab space to set up my own team. I felt like a spoiled child and I am very grateful to Françoise and Jacques for their generous support. Although it was effectively operating as an independent research unit since the end of 2000, my team was officially recognized by the Curie Institute in December 2006 by a 5-year contract.

I started working with Frank Jülicher, who was then working in the same department, immediately after I arrived in Paris. Frank soon left to Dresden to become a director of the Max-Planck-Institute for the Physics of Complex Systems. However, our collaboration survived and is still vivid today. I cannot acknowledge strongly enough how strong Frank's influence has been over the past ten years. The first piece of work that we did together was more related to fundamental physics than to hair-cell physiology. This work was motivated by endless discussions that I had with Jim Hudspeth before leaving New York about finding an unambiguous test to determine whether a noisy signal – here given by the spontaneous fluctuations of hair-bundle position – corresponds to thermal fluctuations or whether it is instead driven by an active (but noisy) process. I had finally come up with the idea to use the fluctuation-dissipation theorem, of which I had heard from Jacques Prost at the time when he was one of my teachers during my Master. The fluctuation-dissipation theorem is a central result of statistical physics that relates, for any system at thermal equilibrium, linear response function and fluctuations. Frank taught me how to apply the theorem to hair cells and together we showed that hair cells evincing spontaneous oscillations of their mechanosensitive hair bundle offer a spectacular example of an active biological system that violates the fluctuation-dissipation theorem (Martin et al., 2001). A hair bundle can oscillate spontaneously or display various forms of mechanical excitability in response to force steps. My first PhD student, Jean-Yves Tinevez (thesis defended in March 2006), combined mechanical stimulation of single hair bundles from the bullfrog's ear with Ca^{2+} iontophoresis to study experimentally how calcium ions control the occurrence of spontaneous oscillations as well as the kinetics and the polarity of active hair-bundle movements (Tinevez et al., 2007). Together with Björn Nadrowski (thesis defended in October 2004), then a PhD student in the group of Frank Jülicher, we built a stochastic theoretical description of active hair-bundle mechanics that can account quantitatively, with only two coupled equations and a minimal number of parameters, for the various incarnations of active hair-bundle motility in hair cells from the frog (Nadrowski et al., 2004; Tinevez et al., 2007). Moreover, this description was successfully extended to other species, including mammals. In collaboration with the group of Christine Petit (Institut Pasteur, Paris), we have recently used the same theory to decipher the functional role of harmonin-b, a protein implicated in a congenital form of deafness, in the transduction machinery of hair bundles from the mouse (Michalski et al., 2009).

Our physical description of active hair-bundle mechanics indicates that oscillatory hair bundles from the bullfrog's sacculus operate near an optimum of mechano-sensitivity but that the maximum sensitivity that a single hair bundle can achieve is seriously limited by intrinsic fluctuations of hair-bundle position (Nadrowski et al., 2004; Jülicher et al., 2009). During his PhD in my group (defence in early 2011) and in close collaboration with the group of Frank Jülicher, in particular with Kai Dierkes (PhD student; thesis defended in 2010), Jérémie Barral showed experimentally that elastic coupling of a hair bundle to neighbors results in effective noise reduction, in turn enhancing the maximal sensitivity that the hair bundle can achieve (Barral et al., 2010). This work was based on a novel dynamic force-clamp procedure in which a hair bundle from the frog was mechanically coupled to two virtual hair bundles resulting from real-time stochastic simulations. In addition, Jérémie has recently studied the response of an oscillatory hair bundle to a two-tone stimulus, *i.e.* a stimulus that contains two frequencies f_1 and f_2. When stimulated near the characteristic frequency of spontaneous oscillation, the hair bundle displays prominent distortion products at linear combinations of f_1 and f_2 as well as partial suppression of the response to a sinusoidal stimulus at f_1 in the presence of a second stimulus at f_2. We interpreted these nonlinear effects, which are also present in the auditory percept of humans, as a necessary price to be paid for the extended dynamical range and the exquisite sensitivity to faint stimuli that is characteristic of vertebrate hearing. This work is unpublished; a manuscript is under preparation.

Active hair-bundle motility by the hair cell, as well as motility and mechanical oscillations in other biological systems, for instance in muscle, rely on the collective action of molecular motors. Since the end of 2004, our team has been developing tools to investigate in vitro the active mechanical properties of molecular motors both for single molecules and small motor assemblies. At the time when we started working on molecular motors, this field was already mature, with renowned researchers that had refined their experimental expertise over many years and exhausted many of the basic questions that one may want to ask about how a molecular motor works. However, although they had been many experiments performed at the single-molecule level or, at the other extreme, with a large number of motors in muscle fibers, comparatively little had been done at the level of small motor collections (= a few tens of molecules) that is relevant for active hair-bundle mechanics. My interest in molecular motors is primarily driven by hearing-related questions. One long-term goal is to understand

the molecular mechanisms by which the vertebrate hair cells set their characteristic frequencies and actively produce oscillatory forces at frequencies that can reach 100 kHz in some mammalian species to achieve exquisite sensitivity and sharp frequency selectivity to weak sound stimuli. Can motor assemblies help? In particular, the exact role played by Ca^{2+} on active force production, which seems essential to produce fast movements in hair-cell bundles, remains to be elucidated. It is plausible, though it remains to be demonstrated, that hair cells use unconventional myosin molecules that can briskly respond to Ca^{2+} changes. During the PhD of Pierre-Yves Plaçais (defended in 2008) and the postdoc of Martial Balland (2004-2006), we used an optical trap to oppose the gliding motion of a single bead-tailed actin filament over a substrate densely coated with myosin-2 molecules and showed that this minimal acto-myosin system can oscillate spontaneously (Plaçais et al., 2009). This finding accords quantitatively with a general theoretical framework, which was introduced by Jacques Prost and Frank Jülicher about 15 years ago while I was doing my PhD, where oscillatory instabilities emerge generically from the collective dynamics of molecular motors under load. In addition we have started probing the dynamical responsiveness of motor assemblies to external mechanical stimuli. These are just preliminary experiments and there is still a long way before we can mimic the workings of the hair bundle's active transduction machinery.

I. INTRODUCTION

1. Psychophysical properties of hearing

At first sight, the vertebrate ear may be viewed as a sort of microphone that responds to sound-evoked mechanical vibrations by producing electrical signals that then propagate along the auditory nerve to the brain. The technical specifications of the human ear are remarkable (reviewed in(Moore, 2004; Hudspeth et al., 2010)). First, our hearing is so sensitive that we can hear sounds that evoke mechanical vibrations of the tympanum comparable to those produced by thermal noise. Second, hearing is so sharply tuned that trained musicians can distinguish tones differing in frequency by only 0.1%. Finally, from the faintest sounds that we can detect near threshold to sounds so intense that they hurt, the sound-pressure level increases by six orders of magnitudes from 20 µPa to 20 Pa. This corresponds to twelve orders of magnitudes of acoustic power! The subjective sensation of loudness spans a much narrower range, a property that justifies the use of a logarithmic unit - the decibel – to measure sound intensity. A tenfold increase in sound-pressure level corresponds to 20 decibels. The smallest intensity difference that can be discriminated for noisy sounds is about 1 dB. The one-millionfold variation of sound-pressure level is thus represented by only 120 units in the decibel scale.

As a consequence of compressive auditory processing, the ear does not work as a high-fidelity sound receiver. As first noted in the 18th century by the Italian violinist Tartini, a person listening simultaneously to two pure tones of frequencies f_1 and f_2 can perceive not only these frequencies but also tones at linear combinations of f_1 and f_2 that are not present in the acoustic stimulus. When the frequency mismatch f_2-f_1 is small ($f_2/f_1 \approx 1.1$), the most prominent "phantom tone" is the cubic distortion product $2{\cdot}f_1$-f_2 (Goldstein, 1967). The nonlinearity that underlies the production of distortions in the auditory percept is extraordinary. First, the cubic distortion product $2{\cdot}f_1$-f_2 persists even for very weak stimuli and is only 15 dB weaker than the primary tones. Second, for two tones of equal intensities, the magnitude of the perceived cubic distortion product increases in proportion to the stimulus, so that their relative level remains nearly constant at 15% over a wide range of stimulus intensities. Finally, the loudness of distortion displays a sharp dependence on the

frequency separation between the two components of the stimulus. In addition to distortions, nonlinear two-tone interference in hearing is also revealed by the phenomenon of suppressive marking, by which the perceived loudness of a tone diminishes in the presence of a second tone at a nearby frequency.

2. The cochlear amplifier:

In humans as well as in the other mammals, the mechano-to-electrical transduction process happens in the cochlea, a fluid-filled tube that takes the shape of a snail's shell (Fig. 1A). Hearing achieves its dazzling characteristics, in particular its wide dynamical range, because the cochlea is endowed with unusual nonlinear mechanical properties (Robbles and Ruggero, 2001). These properties have been characterized over the past 60 years by measuring how the cochlea vibrates in response to sound. As represented schematically in Fig. 1B, the cochlea is split in two compartments by a partition. Although the partition is shown here as a simple line, one should bear in mind that it is in fact a complex structure. In particular, the partition contains sensory *hair cells* that report transverse vibrations to the brain. Remarkably, a sound of a particular frequency elicits significant vibrations of the partition within only a restricted region whose location depends on frequency and whose lateral extension, for faint sound stimuli, spans a few hundred micrometers. High-frequency sounds elicit vibrations near the cochlear base, whereas low-frequency sounds make the partition vibrate significantly near the apex (Fig. 1B). The cochlea thus works as an "acoustic prism" that spatially distributes the energies associated with the frequency components that compose a complex sound to different regions of the cochlear partition. Conversely, when one performs a point measurement along the longitudinal axis of the cochlea, there is a characteristic frequency at which the partition displays a resonance. This resonance can be characterized by measuring the sound intensity that is required to elicit a vibration beyond a given threshold: the partition displays a tuning curve that is sharply peaked at a characteristic frequency (Fig. 1C). When stimulated at resonance, the partition evinces a striking compressive nonlinearity that accommodates the six orders of magnitudes of sound-pressure levels (0-120dB) into only 2-3 orders of magnitudes of vibration amplitudes (Fig. 1D). Over nearly 4 orders of magnitude of sound intensity, the response growth is well described by a power law of power 1/3; the sensitivity, which is determined by dividing the output by the input, correspondingly declines as a power law of

power -2/3. This compressive behaviour contrasts with the linear response that is observed off-resonance. Any transverse section of the cochlea thus displays highly nonlinear mechanical properties, but only near a characteristic frequency.

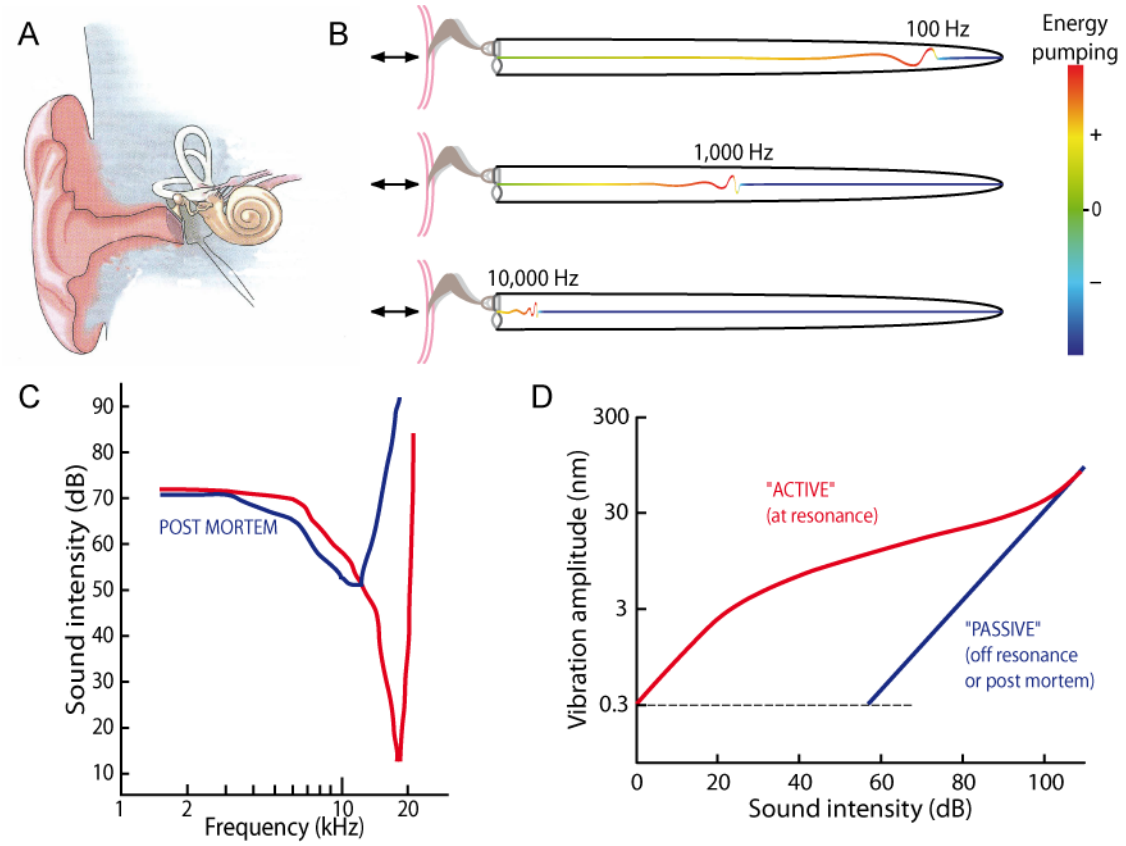

Fig. 1 : Cochlear amplification in mammals. A: Schematic representation of the human ear. A sound-pressure wave evokes vibrations of the eardrum (tympanum) that are transmitted to the cochlea by three ossicles. The cochlea in turn produces electrical signals that travel to the brain along the auditory nerve. Note that the inner ear also mediates the sense of balance through the measurement of head accelerations by the vestibular system. In particular, one notices here three semi-circular canals that are devoted to the detection of rotational accelerations. B: The cochlea, here unrolled and observed in a longitudinal cross-section, is split in two compartments by a deformable partition (multi-colored line). Vibrations of the stapes at a given frequency set the incompressible fluid inside the cochlea into motion. This results in a travelling wave of transverse deformation of the cochlear partition that propagates towards the end (apex) of the cochlea. Each of the 3 diagrams shows the instantaneous position of the partition during the propagation of a traveling wave of the indicated frequency. The color scale portrays the extent of energy pumping that is thought to arise from active force production within the partition. Amplified by the active process, the movement of the cochlear partition grows progressively stronger as the wave approaches a characteristic place, then declines rapidly just before the resonant position associated with the stimulus frequency. Reproduced from (Hudspeth et al., 2010). C: Tuning curve measured at a fixed position along the cochlear partition: the sound intensity that is required to elicit a threshold vibration of 0.35 nm is plotted as a function of frequency. In an active cochlea, a sharp peak is observed at a characteristic frequency, here 18 kHz. Postmortem, the partition is less sensitive to sound by 40-50 dB and is also less-sharply tuned. D: Double-logarithmic plot of vibration amplitude as a function of sound intensity at resonance (red line), i.e. for a stimulus frequency that matches the characteristic frequency of the partition at this location, and off-resonance or post-mortem (dark-blue line). The dotted line marks the threshold of detection (~0.3 nm). Adapted from (Ruggero et al., 1997).

Remarkably, linear mechanics is observed at any frequency when the animal is deprived of oxygen or post mortem. The compressive nonlinearity that is observed in a healthy cochlea is thought to result from a nonlinear and frequency-selective amplificatory process. Amplification should be here understood as an active process that makes use of internal resources of energy of bio-chemical origin to produce mechanical work that compensates for viscous friction and in turn enhances sensitivity to external stimuli. Analysis of the local impedance of the cochlear partition indeed provides strong evidence for negative damping at location basal to the characteristic place at which the partition resonates; energy-consuming elements must pump energy into the vibrating partition (Shera, 2007). By amplifying weak sound-stimuli, this active process reduces by ~50dB the sound intensity that is required to elicit a vibration above the detection threshold, here of about 0.3nm (only!), and thus enormously expands the dynamic range of hearing. By comparing passive (post-mortem) and active tuning curves, one can appreciate that the active process also significantly sharpens frequency selectivity (Fig. 1D).

Perhaps the most compelling evidence that the hearing results from an active process comes from the observation that the ear not only receives sounds but also *emits* sounds, even in the absence of external stimulation. The existence of these spontaneous oto-acoustic emissions suggests that the cochlea can power mechanical oscillations at frequencies within the auditory range, up to 63 kHz in the bat (Kossl and Vater, 1985). To the best of my knowledge, these cochlear oscillations would be the fastest spontaneous mechanical oscillations that are produced in the biological world. Interestingly, spontaneous oto-acoustic emissions have been measured in a wide range of vertebrate species, including frogs, lizards, birds and humans. This suggests that active hearing is ubiquitous in vertebrates and might have originated early in evolution (Manley, 2001). Indeed, although auditory amplification has been most extensively characterized in mammals, other vertebrates can be at least as sensitive and frequency selective. Only mammals, however, can hear at frequencies above ~10 kHz, possibly because their middle ear affords better transmission of air-borne acoustic energy to the inner ear at high frequencies (Manley, 1990). Although the detailed mechanism that would explain how auditory amplification happens is the subject of an intense debate, there is a general consensus that the active process is mediated by action of the ear's mechano-receptive cells, the hair cells.

3. Mechano-electrical transduction by hair cells

3.1 The hair bundle: a mechanical antenna

Hair cells are epithelial sensory cells that each project from their apical surface a stereotypical (and beautiful) hair bundle. The hair bundle is a tuft of a few tens to a few hundreds of actin-filled protrusions, called stereocilia, that are arranged in rows of increasing heights as to form a structure that resembles that of organ pipes in churches (Fig. 2A). The hair bundle is the mechano-sensory organelle of the hair cell. Sound in hearing organs, head acceleration in vestibular organs (sense of balance) and water flow in the lateral line of fish and amphibians ultimately evoke hair-bundle deflections, to which the hair cell responds by generating ionic receptor currents. Mechano-to-electrical transduction, a process that is fast enough to enable the hair cell to respond at auditory frequencies up to ~100 kHz, most probably results from direct mechanical gating of mechanosensitive ion channels, without the intervention of an intermediate enzyme or second messenger. In this scheme, mechanical stimuli affect the extension of elastic mechanical linkages - the "gating springs" - attached to, or part of, the transduction channels.

Stereocilia are interconnected by numerous lateral links (Fig. 2B and C). In particular, the tip of each stereocilium is attached to the flank of the nearest taller neighbor by a single, fine filament called the tip link (Fig. 2C). Tip-link tension controls the open probability of mechanosensitive ion channels that are embedded in the plasma membrane near the tip of the stereocilia. Upon deflection, each stereocilium pivots about its point of insertion at the apex of the hair cell (Fig. 2B). This movement induces shearing between adjacent stereocilia and in turn affects tip-link tension. Although the tip link is ideally placed to constitute the gating spring (Fig. 2D), electron micrographs reveal a structure that is probably too stiff and inextensible. If the tip link is not the gating spring, a compliant linkage would have to be connected in series to the tip link.

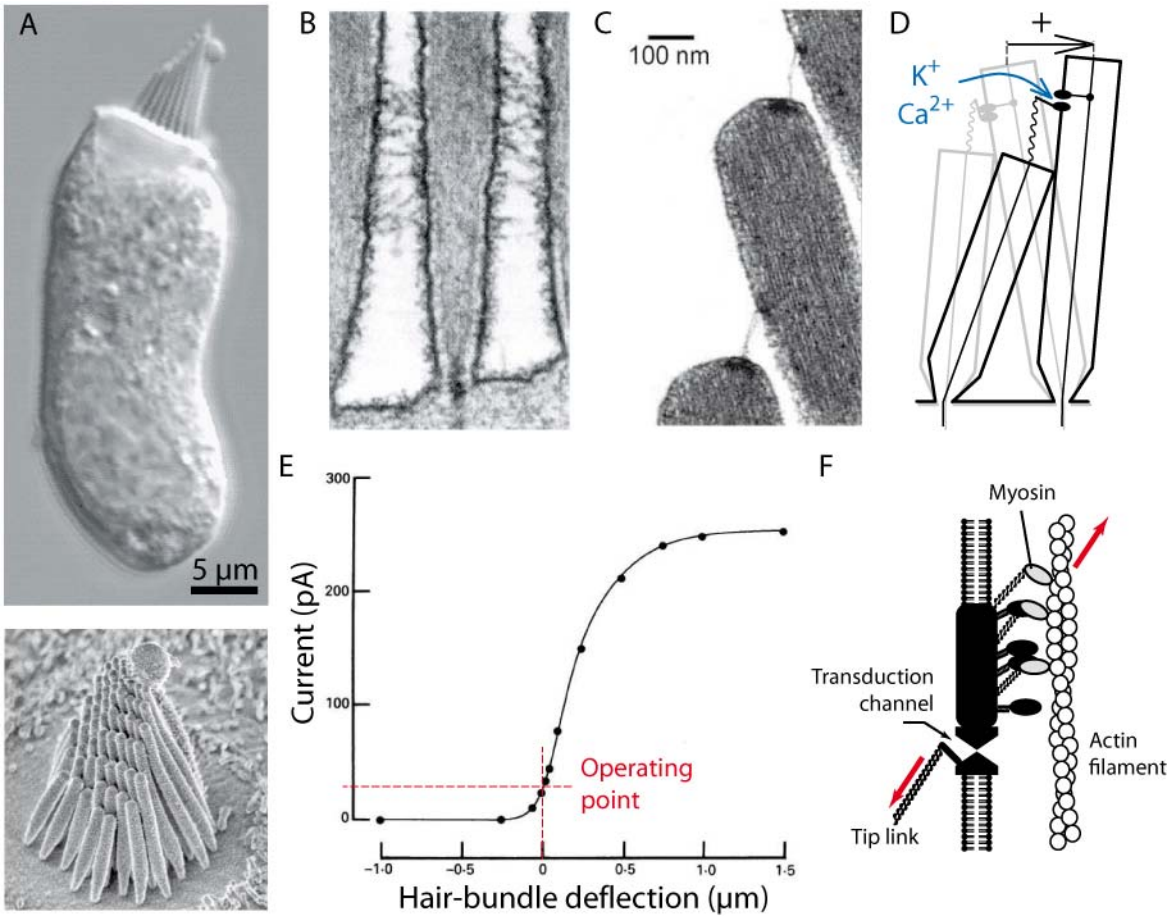

Fig. 2: Hair cell. A : Top : View of a single hair cell extracted from the saccule of the bullfrog (Rana catesbeiana). The apical surface of the cell is adorned by the mechano-sensory hair bundle. Bottom : the hair bundle is composed of a few tens of actin-filled stereocilia that form a staircase pattern. B : Stereociliary pivots. Each stereocilium tapers at its base; only a few tens out of a few hundred actin filaments penetrate into the hair cell, where they form a rootlet. C : Tip links. Each tip link connects the top of a stereocilium to the flank of the nearest taller neighbor. Tension in these oblique links controls the open probability of mechano-sensitive ion channels. D : Gating-spring model of mechano-electrical transduction. A deflection of the hair bundle towards the taller stereocilia, here defined as "positive" (black arrow), raises tip-link tension and evokes an increased influx of K^+ ions, the main ion in the endolymph that bathes the hair bundle, as well as of Ca^{2+} ions. This transduction current evokes a depolarization of the cell's membrane potential, a signal that will eventually initiate release of neurotransmitters at synapses between the hair cell and afferent nerve fibers. E : Sigmoidal relation between hair-bundle deflection and transduction current. The operating point lies in the sensitive region of the relation; a significant fraction of the channels are thus open at rest. F : Functional description of the transduction complex. A few dozens of myosin molecules dynamically anchor the transduction channel to the actin cytoskeleton of the stereocilia. At steady state, the motors are at stall: the force that the motors actively produce towards the top of the stereocilia is balanced by an elastic restoring force in the tip link (red arrows). The motors are thought to respond to changes in tip-link tension and intracellular Ca^{2+} concentration by moving along the actin filaments in an attempt to restore steady-state conditions; this phenomenon is called "mechanical adaptation". Micrographs in A (top), B and C are from Jim Hudspeth. The picture shown in A (bottom) is from Peter Gillespie. The schematic drawing shown in F is adapted from (Hudspeth and Gillespie, 1994).

The transduction currents elicited by a series of step displacements of varying magnitudes describe a sigmoidal relation (Fig. 2E). The range of mechano-sensitivity spans only a few hundreds of nanometers of bundle displacements, which amounts to a couple of degrees of bundle angular deflection. Remarkably, a significant fraction of the transduction channels is open at rest. This condition is necessary for the hair cell to evoke significant receptor currents

in response to small hair-bundle deflections. Chemical disruption of the tip links results in a forward movement of the hair bundle and complete channel closure, which indicates that transduction channels are intrinsically more stable in a closed state. Thus, under control conditions there must be a force-producing machinery that sustains sufficient tip-link tension to position the operating point within the sensitive region of the current-displacement relation. Because each stereocilium is endowed with an actin core, it may not be surprising that myosin motor molecules are involved in maintaining the tip links taut. At steady state, the motors exert an active force directed towards the tip of the stereocilia (where the actin filaments position their barded ends) that is balanced by an elastic restoring force in the tip link (Fig. 2F). Within this framework, the larger the active force that the motors can produce, the higher the open probability P_o of the transduction channels. For sensitive detection of hair-bundle movements, the active motor force must be tightly regulated to impose an open probability that is neither too small ($P_o \cong 0$) nor too large ($P_o \cong 1$). In frog, steady-state tension has been estimated at ~8 pN per tip link at a resting open probability $P_o \cong 0.15$ (Jaramillo and Hudspeth, 1993). A few dozens of non-processive myosin molecules would suffice to sustain this tension. Because the hair bundle comprises ~50 transduction elements (one per stereocilium) that operate in parallel, the total active force that is produced by the motors at stall along the tip-link axis is ~400 pN.

3.2 The motor model of adaptation

Like other sensory cells, hair cells remain sensitive to small, time-varying stimuli even in the presence of a constant background that threatens to saturate the transduction process (Eatock, 2000). This process is called adaptation. In response to a prolonged step displacement of the hair bundle in the positive direction, a hair cell generates a transduction current that first increases in magnitude, reflecting the opening of transduction channels, but then declines with time (Fig. 3). Conversely, a negative bundle displacement elicits first a decrease of the current flowing into the hair cell but at later times, although the bundle position is maintained, the current increases (not shown). Adaptation does not result from inactivation of the transduction channels. Instead, channels reclose when they are opened by a positive step stimulus and reopen for a sustained stimulus of opposite polarity. Note that

adaptation is incomplete: the channels' open probability does not relax completely to its resting value.

If a positive displacement of the hair bundle tenses elastic elements that pull the transduction channels open, then the channels would reclose if tension in these gating springs somehow declined. Conversely, if negative stimulation slackened the gating springs and thus initially closed the transduction channels, channels would reopen if the tension in the gating springs increased. The molecular motors that are associated with the transduction apparatus (fig. 2F) are ideally suited to provide negative feedback on the open probability of the transduction channels. Starting from stall condition, the motors are indeed expected to react to step deflections of the hair bundle by moving along the actin core of a stereocilium until a condition of force balance is restored at steady state (fig. 2F). By increasing tip-link tension, a positive stimulus promotes a slipping motion of the myosins that relaxes the change in tension evoked by the stimulus (Fig. 3A); similarly, a stimulus of opposite polarity would allow climbing of the motor molecules towards the stereociliary tips to rebuilt tension in the tip links (not shown). The implication of myosin Ic in the adaptation process has been carefully tested in the mouse, because the gene encoding for mouse myosin Ic can be mutated. Engineering of an enlarged nucleotide binding pocket in myosin Ic made it possible to specifically block this motor with large ADP analogs (Gillespie et al., 1999). This strategy provided strong evidence that myosin 1c is essential to adaptation, at least in the vestibular system (Holt et al., 2002; Stauffer et al., 2005).

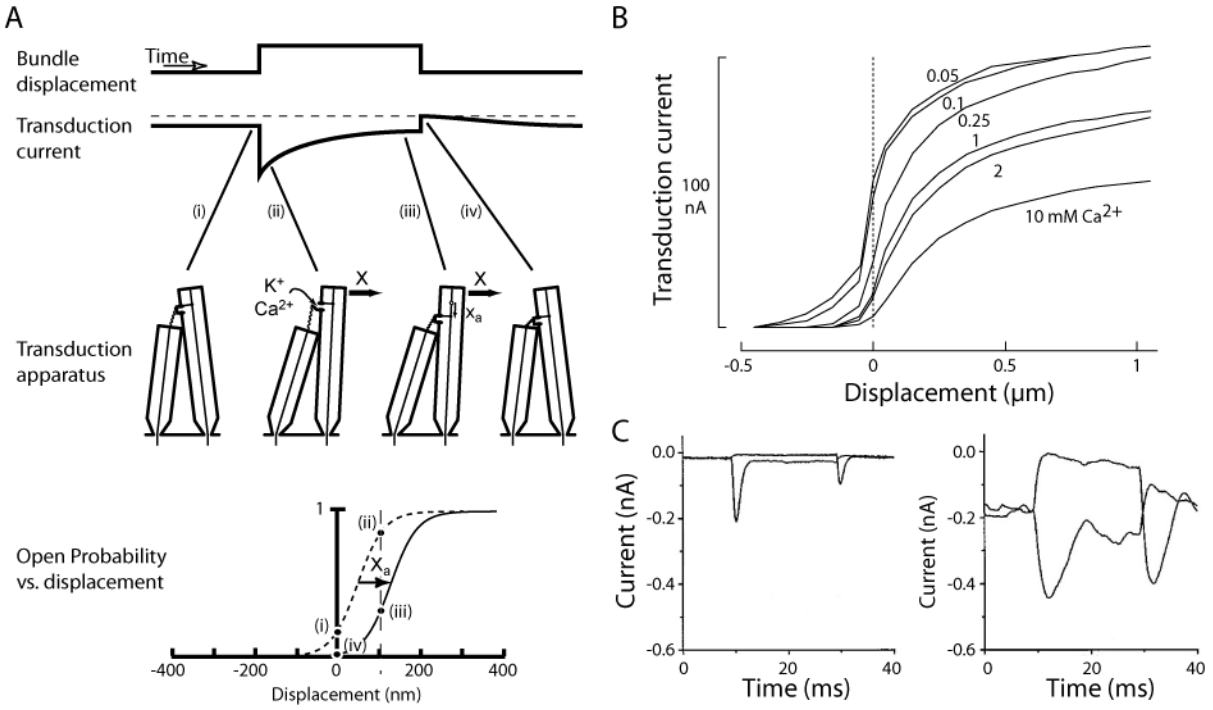

Fig. 3: A : The active-motor model of adaptation. A positive hair-bundle deflection X evokes an inward transduction current which, as adaptation proceeds, declines towards a plateau. Positive stimulation increases tip-link tension and thus fosters opening of the transduction channels. The entry of Ca^{2+} ions in the cytoplasm, together with the increased tension of the tip-link, results in slipping of the myosin molecules towards the base of the stereocilia (vertical arrow) by a distance x_a. This motor movement in turn decreases gating-spring tension, thereby allowing the transduction channel to reclose. Assuming that the transduction channels carry about 15% of their maximal current at rest (point (i)), the abrupt stimulus increases the open probability to a high value (point (ii)). As a result of adaptation and with the bundle clamped at a fixed position of +100 nm, transduction channels reclose (point (iii)). The ensuing decline of the transduction current corresponds to a shift of the open probability-displacement relation along the displacement axis in the direction of bundle movement by a distance $X_a = x_a/\gamma$, in which γ is the geometrical factor that relates hair-bundle deflection to gating-spring extension. (Adapted from Hudspeth and Gillespie, 1994). B and C : The effects of Ca^{2+} on adaptation. Shown here in the bullfrog's saccule (B), the current-displacement curve shifts positively when the Ca^{2+} concentration is increased from 50 µM to 10 mM in the fluid that bathes the hair bundles. Conversely, the proportion of peak current that is activated at rest decreases from 52% in low calcium to 8% or less in high calcium. Note that the magnitude of the maximal transduction current increases when the extracellular calcium concentration decreases. In the turtle's cochlea (C), reducing the calcium concentration from 2.8 mM (left) to 0.05 mM (right) slows down the adaptive decline of the inward transduction current that is produced by +200 nm displacement steps of a hair bundle. A single-exponential fit to the current decay yields here characteristic time constants for the adaptation process of 1.1 ms (left) and 3.5 ms (right). (B is reproduced from Corey and Hudspeth, 1983b; C is adapted from Ricci and Fettiplace, 1998)

3.3 Calcium feedback

Calcium affects the resting open probability of the transduction channels, as well as the kinetics of the adaptation process (Fig. 3B and C). Lower Ca^{2+} concentrations in the endolymphatic fluid that bathes the hair bundles result in higher open probabilities and slower adaptation kinetics. Conversely, higher Ca^{2+} concentrations promote channel closure and fast adaptation. These observations could be explained if Ca^{2+} interacted with the myosin-based

adaptation motor and *decreased* the active pulling force that the motor exert on the tip links (Fig. 2F). Indeed, if the motor is weaker at higher Ca^{2+} concentrations, the channels' open probability is expected to be reduced. In addition, by increasing tip-link tension, a positive stimulus would promote motor slippage towards the base of the stereocilia as well as an increased Ca^{2+} influx through more open transduction channels; if Ca^{2+} rapidly lowered the active force produced by the motors towards the tip of the stereocilia, then the slipping motion of the adaptive motor would be facilitated. By this mechanism, the Ca^{2+} component of the transduction current provides positive electro-mechanical feedback on adaptive motor movements. Adaptation kinetics can then be described by a force-velocity relation that shifts upon Ca^{2+} changes (Fig. 4). In a minimal description of adaptation, the velocity at which the motor can move is linearly related to gating-spring tension and Ca^{2+} only affects the force that the adaptation motor produces at stall. Note that in this case adaptation is complete: any stimulus-evoked change of gating-spring tension can be cancelled by an adaptive motor movement. To accommodate incomplete adaptation, it is usually assumed that each transduction complex is also anchored to the actin cytoskeleton of the corresponding stereocilium by a static elastic linkage, called the extent spring. Although we did include the extent spring in our published description of adaptation (Tinevez et al., 2007), we will ignore it here, for simplicity.

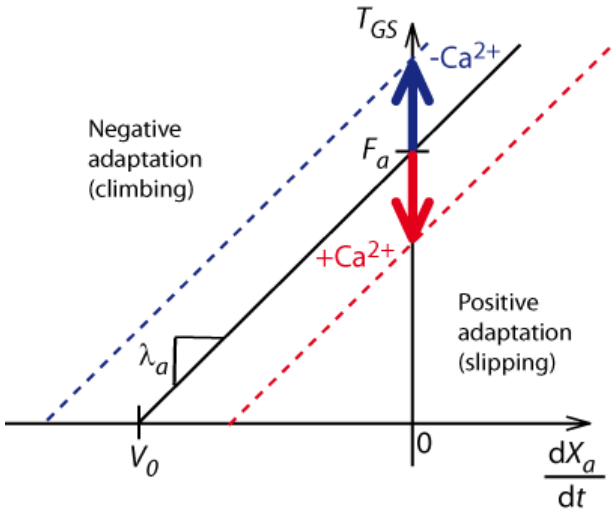

Fig. 4: Physical description of adaptation. The velocity dX_a/dt *at which the adaptation motor moves is linearly related to tension in the gating-springs* T_{GS}*:* $\lambda_a \, dX_a/dt = T_{GS} - F_a$ *. When tension in the gating springs is larger than the motors stall force, the motors slip towards the base of the stereocilia resulting in positive adaptation (*$dX_a/dt > 0$*). In the opposite case, the motors climb towards the top of the stereocila (*$dX_a/dt < 0$*). The motor's stall force* F_a *decreases when the* Ca^{2+} *concentration increases at the intracellular motor site.*

Although other mechanisms are possible, calcium feedback could emerge from a Ca^{2+}-induced reduction of the myosin's duty ratio and thus of the average number of bound myosin molecules at any given time. In agreement with this working hypothesis, some steps in the ATPase cycle of myosin-1c have been shown to be regulated by calcium, resulting in an acceleration of detachment and

a lengthening of the lifetime of the myosin detached state at increased Ca^{2+} concentrations (Adamek et al., 2008). If the transduction channels are somewhat distant from the motor site, as a recent study suggests (Beurg et al., 2009), the kinetics of Ca^{2+} feedback might be limited, at least for high-frequency auditory hair cells, by the diffusion and buffering of Ca^{2+} ions that flow into the cell through these channels. In another model that does not suffer from this limitation, Ca^{2+} ions may bind to the transduction channel (or to a regulatory molecule in its close proximity) to stabilize its closed state. In this case, an increase of the transduction current would directly promote channel reclosure.

4. Methods to probe hair-bundle mechanics

Although I briefly worked during my postdoc with the chicken, the pigeon and even the alligator, all the experiments that I report below were performed on hair cells from an excised preparation of the bullfrog's saccule. This organ of the vestibular system is mainly devoted to the detection of ground-borne vertical acceleration of the head but is also sensitive to low-frequency sounds, within a range of 5-150 Hz. The hair cells are inserted in an epithelium containing ~2,500 cells. The saccular macula sits on a rigid and flat cartilaginous plate that can easily be glued over a 1-mm hole plastic coverslip. This favorable configuration was used to set up a two-compartment chamber that mimics the natural ionic conditions that hair cells experience in vivo where the sensory epithelium separates fluids of differing compositions. The hair-cell somata are immersed in Na^+-rich perilymph whereas the cells' apical surfaces, where hair bundles are situated, are bathed by K^+-rich, Na^+-poor endolymph that is also generally characterized by a reduced Ca^{2+} concentration ($[Ca^{2+}]$~30-300 µM; 250 µM in the frog's sacculus) compared to other extracellular fluids ($[Ca^{2+}]$~1 mM). Controlling the ionic environment around the hair bundle, in particular the Ca^{2+} concentration, proved to be essential to observe some of the features that I describe below, in particular spontaneous hair-bundle oscillations.

Mechanical stimulation of single hair bundles was performed by attaching a flexible glass microfiber to the tip of a hair bundle (Fig. 5). The stiffness of the fiber varied within a range of 0.1-0.5 pN/nm and behaved as a low-pass filter with a cut-off frequency of a few hundred hertz. The position of the fiber's base was controlled by a piezoelectric actuator; the position of the fiber's tip, and in turn of the hair bundle, was measured with nanometer resolution with

a photometric system comprising a photodiode pair. This system allowed force application within a range of 0.1-100 pN. In some experiments, we applied analog or digital feedback between the position of the hair bundle and that of the fiber's base to effectively stiffen the stimulus fiber and in turn clamp the position of the hair bundle. Using this set up, we measured the force-displacement relation of a hair bundle (Martin et al., 2000). We have also recently used feedback to mimic mechanical coupling of a single hair bundle to neighbors (Barral et al., 2010).

Passing a current through a microelectrode – a technique called iontophoresis – allowed local and relatively fast (diffusion limited) application of charged compounds that affects active hair-bundle motility (Ca^{2+}, calcium chelators, channel blockers, etc…).

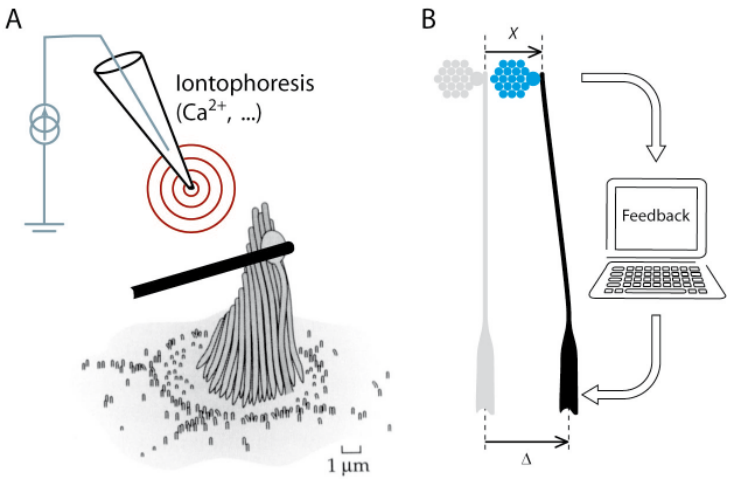

Fig. 5: Hair-bundle stimulation. A: The tip of a flexible glass fiber is affixed to the top of a hair bundle and sticks to the kinociliary bulb. A current passing through a microelectrode expels charged compounds that can affect hair-bundle mechanics. B: A piezo-electric actuator controls the position Δ of the fiber's base. The position X of the hair bundle is measured with photodiodes. The force applied to the hair bundle is proportional to the deflection Δ-X of the fiber. In some experiments, feedback was applied to impose the hair-bundle position to follow a prescribed command signal.

II. ACTIVE HAIR-BUNDLE MOTILITY

The hair bundle is more than a passive receptor – a mechanical antenna – whose mechano-sensitivity would solely result from coupling ion channels to elastic gating springs. Because the gating springs are dynamically anchored to the actin cytoskeleton of the stereocilia by molecular motors and Ca^{2+} influx through open transduction channels provides electro-mechanical feedback on gating-spring tension, the hair bundle is an active mechanical structure which, similarly to a muscle, can convert energy of biochemical origin (ATP hydrolysis, Ca^{2+} binding/unbinding) to produce mechanical work. The most striking manifestation of active hair-bundle motility comes from the observation of spontaneous oscillations. A hair bundle can also be quiescent but display various forms of mechanical

excitability in response to force steps. I describe below the conditions under which these different classes of motility are observed and show that they can all be described by a simple physical description of the interplay between mechano-electrical transduction, the activity of the adaptation motor and Ca^{2+} feedback.

1. Spontaneous hair-bundle oscillations

This section describes work that was performed during my postdoc with Jim Hudspeth, although we further studied spontaneous oscillations during the PhD of Jean-Yves Tinevez in my group, in particular to clarify the role played by Ca^{2+} (Section II.3).

1.1 Oscillation properties

By placing the sensory epithelium in a two-compartment chamber, it is possible to mimic the peculiar ionic environment that hair cells experience in vivo, in particular the relatively low Ca^{2+} concentration (250 μM for this species) in the artificial endolymph that bathes the hair bundles. Under such ionic circumstances, free-standing hair bundles from the bullfrog's saccule routinely display spontaneous oscillations at 5-75 Hz with peak-to-peak magnitudes as large as 80 nm (Martin et al., 2003). The bundle's motion is not sinusoidal but instead resembles the relaxation oscillations observed in various dynamical systems: in each half cycle, a slow excursion in one direction is interrupted by an abrupt jump in the opposite direction. As a consequence the probability distribution of the bundle's position is bimodal and hair-bundle dynamics is well approximated by a two-state description (Clausznitzer et al., 2008). The spectral density of each oscillation displays a clear peak centered at a frequency f_C that defines the characteristic frequency of the oscillation (Fig. 6A). The regularity of an oscillation is characterized by the quality factor $Q = f_C / \Delta f \cong 1-3$, in which Δf is the width of the spectrum at half its maximal value. The hair-bundle movement thus looses phase coherence after a couple of cycles of an oscillation only; oscillations are noisy (Martin et al., 2001).

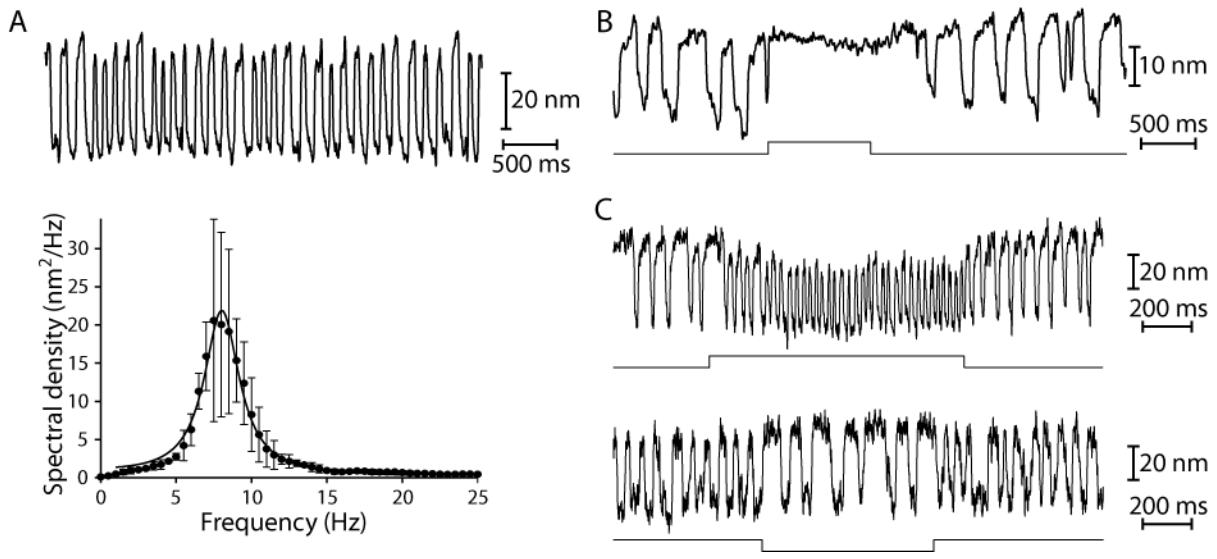

Fig. 6: A: Spontaneous hair-bundle oscillation and corresponding power spectrum. B: Effect of transduction channel blockage by an iontophoretic pulse of gentamicin (shown below). C: Effect of a local increase (top) or decrease (bottom) of the Ca^{2+} concentration on a spontaneous hair-bundle oscillation from iontophoresis of Ca^{2+} or of a Ca^{2+} chelator, respectively. Data shown in A from (Martin et al., 2001) and in B from (Martin et al., 2003).

Spontaneous hair-bundle oscillations rely on functional mechano-to-electrical transduction (Martin et al., 2003). Blocking the transduction channels by iontophoresis of gentamicin, a molecule known to plug the channel's pore, indeed reversibly stops the oscillation (Fig. 6B). However, a hair bundle can oscillate spontaneously when the membrane potential of the hair cell is clamped (no receptor potentials) or when K^+, the cation in the endolymph that carries most of the transduction current in vivo, is replaced by a big non-permeant cation. Only the calcium component of the transduction current appears to play an essential role in the generation of spontaneous hair-bundle oscillation (Fig. 6C). When the Ca^{2+} concentration in endolymph exceeds ~1 mM or falls below ~100 µM, the oscillations disappear. With an oscillatory hair bundle, transiently elevating the Ca^{2+} concentration by Ca^{2+} iontophoresis increases the oscillation frequency. Reducing the Ca^{2+} concentration through the iontophoretic application of a Ca^{2+} chelator has the opposite effect. In addition, quiescent hair bundles can sometimes be brought into oscillation by locally increasing the Ca^{2+} concentration (see Fig. 9A in Section II.3, page 35). Clearly, calcium in the artificial endolymph that bathes the hair bundles acts as a control parameter of a bundle's dynamic behavior (Martin et al., 2003; Tinevez et al., 2007).

Most hair bundles are normally attached to an overlying gelatinous structure and must thus operate against a mechanical load. Using partial displacement clamping to increase the

effective stiffness of the stimulus fiber attached to a bundle, we observed that the characteristic frequency of spontaneous oscillation increases, the magnitude of oscillation declines and the oscillation become more irregular (Martin et al., 2003). A sufficiently great increase in the effective stiffness of the stimulus fiber suppresses well defined bundle oscillations altogether.

1.2 Negative stiffness

Using a displacement-clamp procedure (Fig. 5), one can effectively stiffen the flexible fiber to which a hair-bundle is attached and keep a hair bundle still, even if the bundle oscillates spontaneously under control conditions. From this reference position of zero external force (by convention), we then measure the force that must be applied to the hair bundle to impose a step deflection of varying magnitude (Martin et al., 2000). The bundle's elastic properties are usually assayed by doing the measurement as quickly as possible after the bundle has been abruptly deflected, in practice a few milliseconds after the stimulus onset. This delay is long enough to ensure that transduction channels have time to fully respond to the stimulus and that the viscous hydrodynamic drag that necessarily impedes abrupt bundle motion has vanished. The delay is also generally short enough to avoid significant development of the adaptation process. When displaced extensively either in the positive or in the negative direction, the hair bundle behaves as a linear spring of constant stiffness. For intermediate displacements, however, the hair bundle appears to be softer. Remarkably, in the case of an oscillatory hair bundle, there is a region of the force-displacement relation where the slope is negative (Fig. 7A).

Nonlinear force-displacement relations had been observed earlier in the saccule of the bullfrog under different ionic conditions (Howard and Hudspeth, 1988) as well as in the cochlea of the turtle and in the vestibule and the cochlea of the mouse (Russell et al., 1992; Géléoc et al., 1997). In all these case, however, the hair-bundle stiffness remained positive at all deflections. It was shown that the hair bundle is more compliant over the narrow range of hair-bundle deflections that elicits significant channel gating. Moreover, blocking the transduction channels with gentamicin abolishes the position-dependent stiffness, including negative stiffness: with channel's blocked, the force-displacement relation is linear (Fig. 7B).

The reduction in stiffness upon channel gating can readily be interpreted with the gating-spring model of mechano-to-electrical transduction (Fig. 2D). Mechanical activation of the transduction channels indeed dictates a reciprocal relationship between gating of the transduction channels and tension in the gating springs. An external force in the positive direction will evoke an increase of the channels' open probability; channel opening reduces the extension of the gating spring thereby generating an effective "gating force" in the positive direction. Conversely, a negative force closes channels; channel closing in turn produces a force in the negative direction. Along the axis of a gating spring, gating of a single channel produces a gating force $z = k_{GS}\ d$, where k_{GS} is the gating-spring stiffness and d is the gating swing, *i.e.* the size of the conformational change associated with channel gating (Fig. 7C).. Because the gating force provides an extra give in the direction of the applied force, the stiffness of the transduction apparatus will be lower than that of the gating spring alone, a process termed "gating compliance" (Howard and Hudspeth, 1988). It is accordingly expected that the stiffness of the hair bundle depends on the open probability of the transduction channels and thus on hair-bundle displacement (Fig. 7D).. The force-displacement relation F-X can be described by a simple nonlinear equation:

$$F = \mathrm{K}_\infty X - NZ P_o + F_o , \qquad (1)$$

in which $P_o = 1/\left(1+\exp\left(-Z\left(X - X_0\right)/\left(k_B T\right)\right)\right)$ is the open probability of the transduction channels (a sigmoidal function of X), K_∞ is the hair-bundle stiffness when channels are either all closed or all open (P_o=0 or P_o=1 respectively), N is the number of transduction elements operating in parallel, Z is the single-channel gating force and F_o is a force offset. Note that the single-channel gating force $\mathrm{Z} = \gamma\,\mathrm{z}$, here expressed along the horizontal stimulation axis (Fig. 5), is related to the gating force z along the tip-link axis by a geometrical projection factor γ. The stiffness $\mathrm{K}_\infty = \mathrm{K}_{SP} + \mathrm{K}_{GS}$ can be written as the sum of a contribution $\mathrm{K_{SP}}$ coming from all the stereociliary pivots and a contribution $\mathrm{K_{GS}}$ that describes the combined gating-spring stiffness. The first contribution is defined as the hair-bundle stiffness when the tip links are severed; $\mathrm{K_{SP}}$ represents only 20-30% of the overall stiffness. Negative stiffness is expected to arise is gating compliance is strong enough that

$$Z D P_o\left(1 - P_o\right) > \left(1 + \mathrm{K}_{SP}/\mathrm{K}_{GS}\right) k_B T . \qquad (2)$$

Experimental force-displacement relations are well described by Equation 1, which yields $Z \cong 0.7$ pN, $K_\infty \cong 0.7$ pN/nm and $N \cong 50$. From these numerical values, we then estimate that the conformational change associated with channel gating can be as large as ~10 nm! This value is too large to simply reflect the movement of a channel's pore-obstructing gate. The molecular origin of the conformational change associated with channel gating thus remains mysterious. The mechanical operating point of the hair bundle can be defined as the origin of the relation ($F = 0$; $X = 0$). For an oscillatory hair bundle, the operating point sits near the center of the negative-stiffness region, corresponding to an open probability $P_o \cong 0.5$.

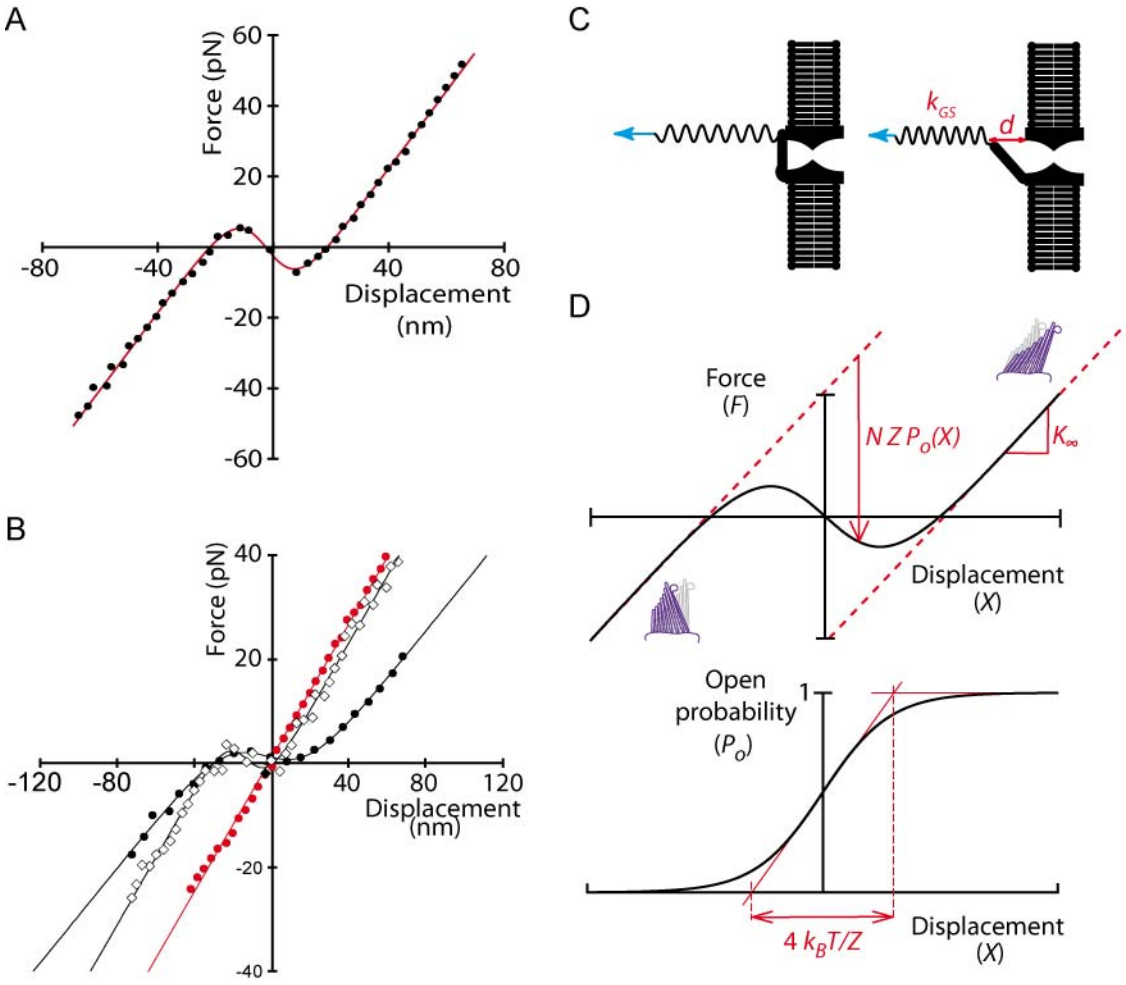

Fig. 7: Negative hair-bundle stiffness. A: Force-displacement relation of an oscillatory hair bundle. The operating point (F = 0; X =0) is near the center of the relation. The red line corresponds to a fit by Equation 1 given in the text. B: In the presence of gentamicin, a drug that blocks transduction channels, the force-displacement relation of a hair bundle that normally displays negative stiffness (black disks) becomes linear (red disks). Negative stiffness is restored in gentamicin-free endolymph (white disks). C: Gating swing and gating force. Opening (respectively, closure) of a transduction channel is associated with a reduction (respectively, increase) of gating-spring extension by a distance "d". Tension in the gating-spring (cyan) thus decreases by an amount $z = k_{GS} d$ upon channel opening, and increases by the same amount upon channel

closure. D: The gating-spring model associates the reduction of hair-bundle stiffness (top) to the open probability of the transduction channel (bottom). When the channels are all closed or all open, the hair bundle behaves as a linear spring of stiffness K_∞ *. The plots indicate how the force-displacement relation is shaped by the mechanical correlate of channel gating. The force* $N Z P_o(X)$ *indeed represents the average gating force produced by channel opening when the hair bundle is brought to a position X from an initial position at which all channels are closed. The single-channel gating force* $Z = \gamma z$ *is measured along the stimulation axis and related to the gating force z along the tip-link axis by a geometrical projection factor* γ*. The larger the single-channel gating force Z, the more pronounced is the effect of gating compliance on hair-bundle stiffness. All positions of negative stiffness are unstable. Data shown in A from (Martin et al., 2000) and in B from (Martin et al., 2003).*

2. "Excitable" hair bundles – Mechanical correlates of adaptation

With hair cells immersed in a standard saline containing calcium in the millimolar range, transduction channels display a low open probability at rest (Fig. 2E) and hair bundles are most often quiescent. When subjected to an abrupt step force in the positive (=excitatory) direction, however, the hair bundle first moves in the direction of the applied force but can then displays a transient movement in the opposite direction called the "twitch" (Fig. 8A). This movement in opposition to the external force is associated on a similar timescale with reclosure of the transduction channels (Howard and Hudspeth, 1987; Ricci et al., 2000), a process often called fast adaptation because it happens on a millisecond (or less in other species) timescale. A second component of adaptation has been distinguished in the transduction current by a relaxation time that is one or more orders of magnitude longer than that characteristic of fast adaptation. Slow adaptation is correlated with a hair-bundle movement of similar time course but of directionality opposite that of the recoil seen in twitches. Under these conditions, negative (=inhibitory) stimuli elicit slow monotonic hair-bundle movements in the direction of the applied force as well as a slow and monotonic adaptive current decline.

At relatively low Ca^{2+} concentrations (≤250 µM), a situation that favors high open probability of the transduction channels (Fig. 2E), quiescent hair bundles can also display non monotonic movements in response to force steps, but only in response to negatively directed stimuli (Fig. 8B). These "negative twitches" (Tinevez et al., 2007) differ from those elicited by positive stimulation by their slower kinetics and often resemble one cycle of spontaneous oscillation. As would be anticipated from the gating-spring model (Fig. 7D) if the transduction channels, under resting conditions, were mostly closed in one case and mostly open in the other, the two types of twitches are associated with force-displacement relations

that are centered at displacements of opposite signs with respect to the mechanical operation point ($F = 0$; $X = 0$). Although these relations always present a restricted region of reduced slope, twitches are not necessarily associated with the presence of negative stiffness. Twitches are observed when the external force step has the right polarity to impose a displacement of the hair bundle within or beyond the compliant region of the corresponding force-displacement relation, and thus to evoke significant channel gating.

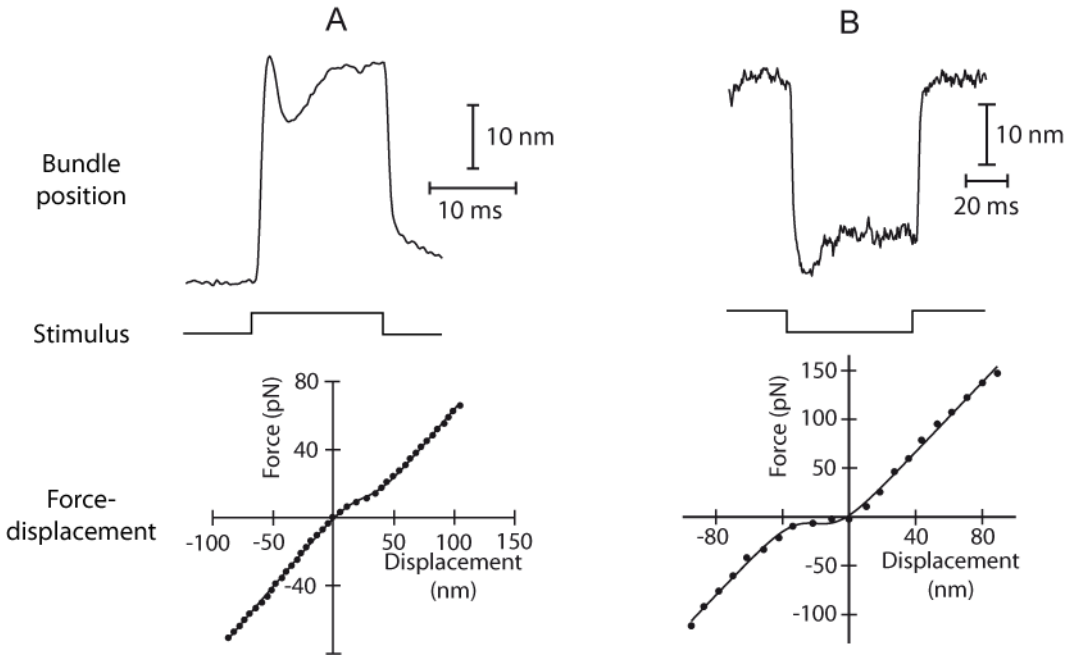

Fig. 8: Mechanical excitability. A: A hair bundle with the force-displacement relation shown at the bottom displayed a twitch (top) in response to a positive step displacement of the stimulus fiber's base (middle). Note that there is no region of negative stiffness in the force-displacement relation. B: Twitch in response to a negatively-directed stimulus for another hair bundle. In both cases, the hair bundle displays a transient recoil; no recoil is observed for stimuli of opposite polarity (not shown). The Ca^{2+} concentration in the fluid that bathes the hair bundles is 4 mM and 250 µM in A and B, respectively. Adapted from (Tinevez et al., 2007).

3. Calcium control of active hair-bundle motility

As already mentioned for spontaneous oscillations, Ca^{2+} affects the kinetics of active hair-bundle movements. Twitches are sharper at higher Ca^{2+} concentrations and correspondingly broader at lower Ca^{2+} concentrations. Calcium also controls the type of movement that can be observed by affecting the resting open probability of the transduction channels (Fig. 2E) and in turn the operating point of the hair bundle within its force-displacement relation (Fig. 8). Large enough Ca^{2+} changes elicit transitions between the three classes of active hair-bundle motility, from spontaneous oscillations to positive or negative twitch, or from quiescence to

spontaneous oscillations (Fig. 9A). These transitions are associated with Ca^{2+}-evoked shifts of the force-displacement relation (Fig. 9B).

The essential role played by Ca^{2+} in active hair-bundle motility is further demonstrated by measuring the hair-bundle movements that are evoked by iontophoretic pulses of Ca^{2+} or of a Ca^{2+} chelator (Fig. 9C-E). Remarkably, the directionality of the response can be reversed by applying a static position bias to the hair bundle; this polarity reversal is then associated with a significant change in the kinetics of motion. The Ca^{2+} component of the transduction current can thus have opposite effects on gating-spring tension. Note that because adaptation is incomplete, a static bias of hair-bundle position is expected to change the operating point of the hair-bundle within its nonlinear force-displacement relation. These observations again (Fig. 8) suggest that the operating point controls directionality and kinetics of active hair-bundle movements.

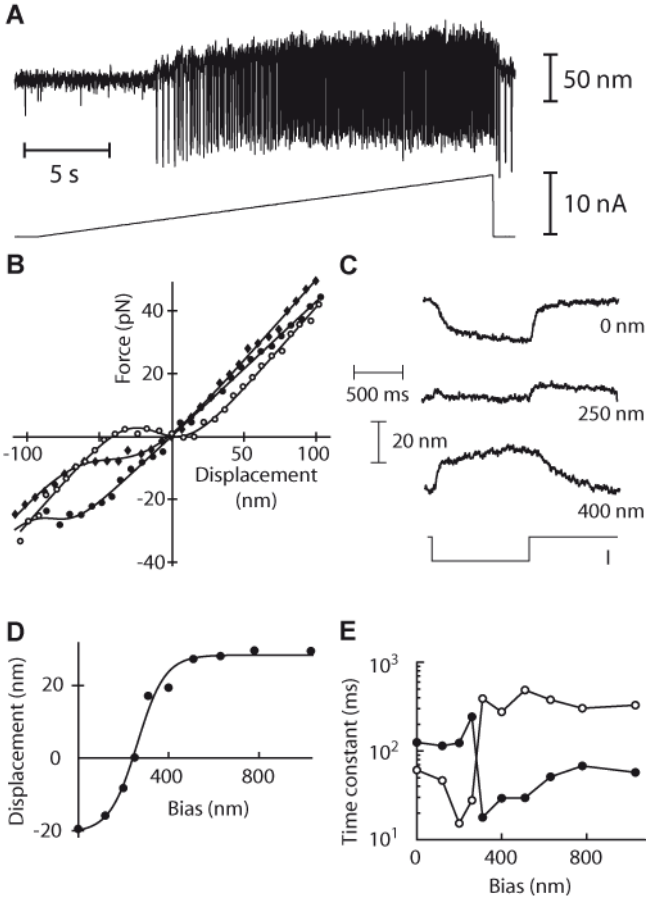

Fig. 9: Ca^{2+} effects. A: From quiescence to spontaneous oscillation with Ca^{2+} iontophoresis. At a critical value of the iontophoretic current and thus of the extracellular Ca^{2+} concentration, the hair bundle displays an oscillatory instability, called Hopf bifurcation. B: Ca^{2+} iontophoresis evokes a positively-directed shift of the force-displacement relation. This hair bundle was quiescent under control conditions (black disks), and for moderate Ca^{2+} pulses (black diamonds) but started oscillating spontaneously when the Ca^{2+} concentration was raised enough to bring the bundle's operating point within a region of negative stiffness (white disks) B: Hair-bundle movement evoked by an iontophoretic pulse (shown at the bottom) of a Ca^{2+} chelator. The stimulus evoked a negatively directed and slow hair-bundle-movement movement under control conditions but a movement of opposite directionality and of faster kinetics when the hair-bundle resting position had first been subjected to a static bias of +400 nm. C: Hair-bundle displacement at steady state as a function of the magnitude of the position bias. D: Time constant of hair-bundle motion at the onset (black disks) and offset (white disks) of the stimulus as a function of bias. Reproduced from (Tinevez et al., 2007).

Experiments from both this Section and Section II.4.1 were performed by Jean-Yves Tinevez during his PhD in my group.

4. Physical description of active hair bundle motility

In collaboration with the group of Frank Jülicher, we have developed a minimal physical description of active hair-bundle mechanics (Fig. 10) that takes into account three ingredients only: (i) a force-displacement relation that contains a region of reduced slope as the result of gating compliance, (ii) adaptation motors that exert an active force against elastic gating springs and (iii) electro-mechanical feedback by the Ca^{2+} component of the transduction current on the force that the adaptation motor can produce (Nadrowski et al., 2004; Tinevez et al., 2007). The waveform and kinetics of active hair-bundle movements result from a dynamic interplay between the positions X of the hair bundle and X_a of the adaptation motor that obeys two coupled first-order differential equations:

$$\lambda \frac{dX}{dt} = -T_{GS}\left(X, X_a\right) - \mathrm{K}_{SP} X + F\,, \tag{3}$$

$$\lambda_a \frac{dX_a}{dt} = T_{GS}\left(X, X_a\right) - F_a\,. \tag{4}$$

The external force F is applied at the hair bundle's top along the horizontal axis of a hair bundle's vertical plane of bilateral symmetry (Fig. 5). All variables are here expressed along this axis. The open probability $P_o = 1/\left[1 + A\exp\left(Z\left(X - X_a\right)/\left(k_B T\right)\right)\right]$ of the transduction channels is a sigmoidal function of the relative position between the hair bundle and the adaptation motor, where Z is the single-channel gating force and $1/(1+A)$ is a constant that represents the channels' open probability when the tip links are severed. Equation 3 describes the dynamical behaviour of the hair-bundle position X in response to the external force F. The hair bundle moves at a velocity that is inversely proportional to the friction coefficient λ. At steady state ($\mathrm{d}X/\mathrm{d}t = 0$), F is balanced by the sum of the elastic restoring force $\mathrm{K}_{SP}X$ provided by the stereociliary pivots and the total tension $T_{GS} = \mathrm{K}_{GS}\left(X - X_a - D\,P_o\right)$ in the gating springs. At a fixed position X_a of the motors, this force-displacement relation matches that given by Equation 1 in Section II.1.2 and shows gating compliance. Measurements of this relation (Fig. 7) provide numerical estimates for the combined stiffness K_{GS} of the gating springs and K_{SP} of the stereociliary pivots as well as of the gating swing D. Equation 4 describes the dynamical behaviour of the adaptation motor by a linear force-velocity relation of slope λ_a (Fig. 4). At stall ($\mathrm{d}X_a/\mathrm{d}t = 0$), the active motor force F_a is balanced by tension in

gating springs. Here, we neglect static linkages between the transduction apparatus and the actin cytoskeleton of the stereocilia that may limit the extent of adaptation; in this version of the model, adaptation is complete.

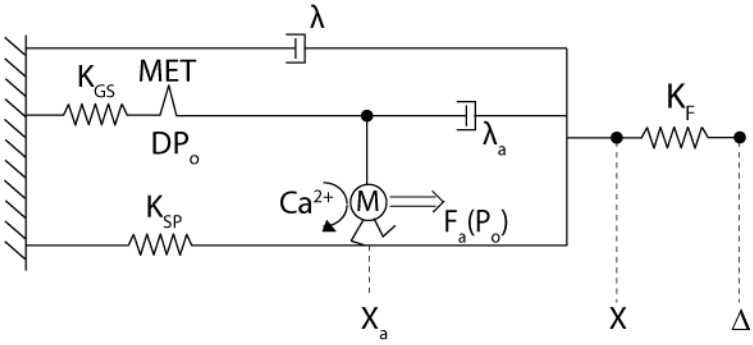

Fig. 10: Hair-bundle model. Transduction elements are connected to gating springs of combined stiffness K_{GS} and dynamically anchored to the actin cytoskeleton of the stereocilia by adaptation motors (M) that can change their position X_a. A rapid change in position X of the hair bundle affects tension in both gating and pivot springs, the later being of combined stiffness K_{SP} and operating in parallel to the former. The speed of hair-bundle motion is inversely proportional to the friction coefficient λ. Opening of a transduction channel (MET) evokes a decrease of gating-spring extension that amounts to a motion of size D at the bundle's top. When tension in the gating springs differs from the active force F_a that the adaptation motors produce at stall, the motors are moving. Motor speed is inversely proportional to λ_a, which represents the slope of the force-velocity relation of the motors. The motor force F_a is down regulated by the Ca^{2+} component of the transduction current. Gating-spring tension, which controls the channels' open probability P_o, is a function of the relative position X-X_a between hair bundle and motors. The stimulus fiber is represented by a spring of stiffness K_F; the position of its base is Δ.

Important simplifying assumptions in the description concern the effect of Ca^{2+} on adaptation: we assume both that the motor's stall force F_a varies linearly with the Ca^{2+} concentration at the motor site and that a change in the channel's open probability evokes an instantaneous change of this concentration. We can then write:

$$F_a \cong F_{MAX}(1 - SP_o), \tag{5}$$

where S and F_{MAX} are two control parameters that represent the Ca^{2+}-feedback strength on the motor force and the maximal force that the motors can produce, respectively. Note that S is proportional to the Ca^{2+} concentration in the fluid that bathes the hair bundles and that the only nonlinearity in the model comes from the sigmoidal functional form of the open probability P_o. Despite its relative simplicity, this description accounts quantitatively for the various forms of active hair-bundle motility that can be observed with hair cells from the bullfrog's saccule (Fig. 11). Moreover, this description also applies to complex active hair-bundle movements that were observed by others in the cochlea of the turtle and the rat (Tinevez et al., 2007). Our results thus suggest that hair cells from different species might use a conserved mechanism of active force production by their hair bundle. Simulations were performed by Jean-Yves Tinevez during his PhD

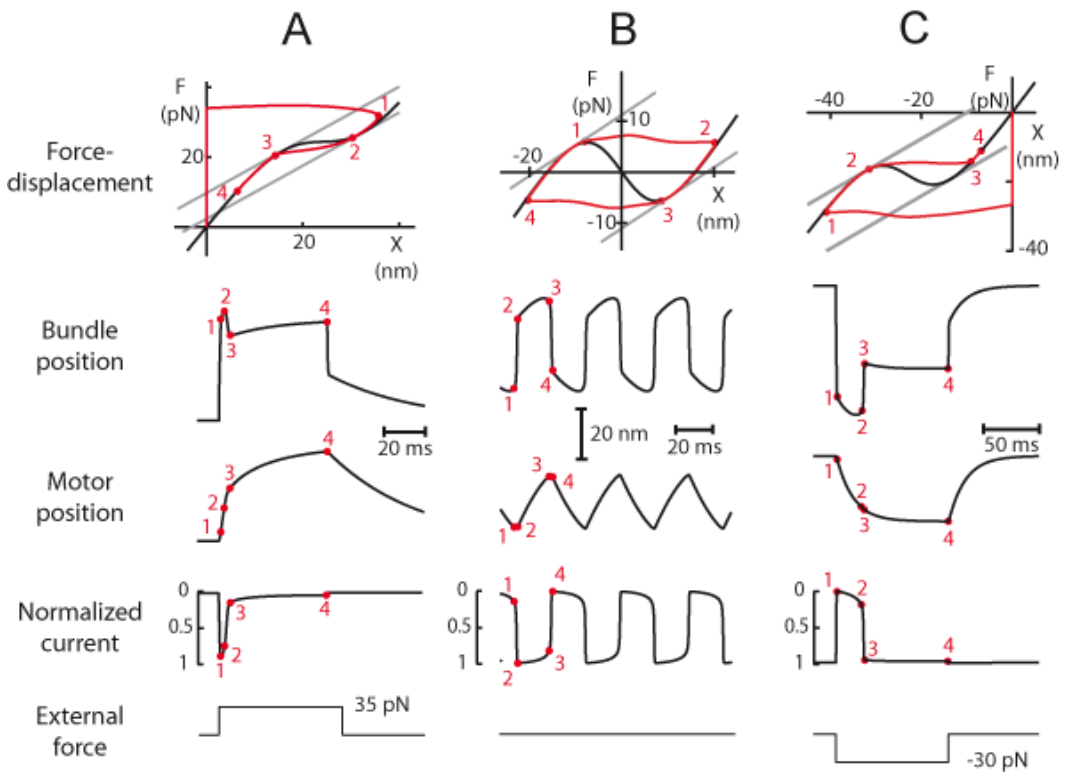

Fig. 11: Simulations of active hair-bundle movements. A: Positive twitch. B: Spontaneous oscillations. C: Negative twitch. The line in red represents the trajectory of the hair-bundle within its intrinsic force-displacement relation. Note that the non monotonic twitches shown in A and C are produced by a monotonic motion of the adaptation motor. Reproduced from (Tinevez et al., 2007).

4.1 Twitch

In the case of a quiescent hair bundle, force steps evoke monotonic adaptive movements of the adaptation motor that can be associated with non-monotonic movements of the hair bundle. The complexity of active hair-bundle motility results from a nonlinear and dynamic tradeoff between opposing forces that are produced by movements of the adaptation motor on the one end and those resulting from channel gating on the other end. The motor works to cancel any change in gating-spring tension that is evoked by external stimulation and thus promotes hair-bundle movements in the direction of the stimulus. For instance, the increased gating-spring tension that results from a positive stimulus evokes an adaptive slipping motion of the motor that decreases tension, thereby allowing the hair bundle to move further in the positive direction (Fig. 12A). The adaptive change in gating-spring tension, however, will also prompt rearrangements of the transduction channels and in turn internal forces. Channel reclosure during adaptation to a positive force step increases gating-spring tension and thus favors negative hair-bundle movements (Fig. 12B). Conversely, reopening of the transduction

channels that were closed by a negative stimulus yields a decrease of gating spring tension and foster positive bundle movements. Hair-bundle movements in opposition to the stimulus are thought to be produced by internal forces that result from conformational changes associated to channel gating during adaptation. The strength of adaptive gating forces depends on the bundle's operating point; it will be maximal for a channels' open probability $P_o = 0.5$ and always negligible for $P_o \cong 0$ or $P_o \cong 1$. A recoil is observed if gating compliance is strong enough that

$$Z D P_o(1 - P_o) > k_B T \,, \tag{6}$$

where Z and D are the single-channel gating force and gating swing, respectively (Fig. 7). Note that this condition is less restrictive than the condition of negative stiffness given by Equation 2. The condition expressed by Equation 6 is indeed satisfied if there exists a region in the force-displacement curve of the hair bundle where the local slope is smaller than the stiffness K_{SP} of the pivots (≅+200 μN/m in the bullfrog's saccule).

In addition, the Ca^{2+} component of the transduction current provides positive electrical-to-mechanical feedback on adaptive motor movements and in turn increases adaptation kinetics. If the Ca^{2+}-feedback strength is large enough that $SF_{MAX} > K_{GS} D$ (Fig. 12C), a condition that is favored by high Ca^{2+} concentrations, adaptation can be fast (~1 ms timescale) near $P_o = 0.5$ but is comparatively slower when $P_o \cong 0$ or $P_o \cong 1$ (~10 ms timescale). For weak Ca^{2+} feedback ($SF_{MAX} < K_{GS} D$), adaptation is instead very slow (~100 ms timescale or more) near $P_o = 0.5$ (Fig. 12D). Note that calcium feedback does not affect adaptation kinetics when transduction channels are near all open or all closed.

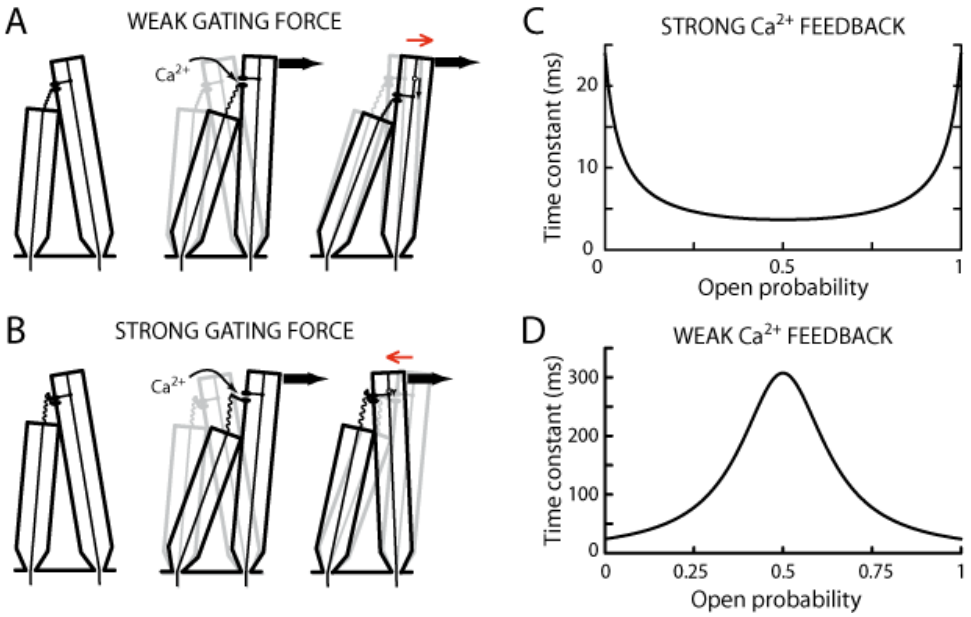

Fig. 12: Qualitative description of adaptive hair-bundle movements. A: When adaptive movements of the motor (vertical arrow) evoke weak gating forces, the hair bundle (red arrow) moves in the direction of the stimulus (thick black arrow). This happens when the hair bundle operates near a channels' open probability of $P_o \cong 0$ or $P_o \cong 1$, or if the single-channel gating force is too small. B: If instead a movement of the motor evokes large gating forces, the hair bundle moves in a direction opposite that of the stimulus. C and D: In response to small hair-bundle deflections, the time course of adaptive motor movement is exponential. The time constant of adaptive motor movements is here plotted as a function of the channels' open probability at rest. With strong Ca^{2+} feedback (C), adaptation can be fast near $P_o = 0.5$. Parameters are the same as in Figure 11A ($S = 3.8$; $SF_{MAX} > K_{GS}D$). With weak Ca^{2+} feedback (D), adaptation is instead very slow. Parameters are the same as in C but with a reduced Ca^{2+}-feedback strength $S = 0.25$ ($SF_{MAX} < K_{GS}D$).

4.2 Spontaneous oscillation

Positions of negative stiffness are unstable. A free or weakly loaded bundle cannot settle there, for any mechanical perturbation will eject the hair bundle to a position of force balance in a flanking region of positive stiffness. Because of the intimate relation between hair-bundle mechanics and channel gating, there is thus a whole range of open probabilities at which the hair bundle cannot be at steady state. The channels' open probability is set by the Ca^{2+}-regulated active force that the adaptation motor can exert at stall on the gating springs. A stable steady state will be out of reach if this force corresponded to an unstable open probability of the transduction channels, for instance $P_o = 0.5$. By this (qualitative) mechanism, the hair bundle is driven into spontaneous oscillations by the adaptation motor, because the motor is perpetually frustrated in its attempt to reach a thermodynamically unstable position (Fig. 11B).

5. Using modeling to decipher the functional role of a protein expressed by a "deafness gene" in the transduction machinery.

In collaboration with the group of Christine Petit (Institut Pasteur, Paris), we have recently used our theoretical description of hair-bundle mechanics to shed light on the possible role played by the protein harmonin-b in the transduction machinery of the hair bundle. Harmonin is a submembranous protein that is encoded by the gene responsible for Usher syndrome type1C (USH1C), a disease characterised by congenital profound deafness, vestibular dysfunction and delayed onset retinopathy leading to blindness. Harmonin-b is located at the upper insertion point of the tip links. In mutant mice lacking harmonin-b, adaptation of the transduction currents to static deflection of the hair bundle shows increased speed and extent in utricular hair cells, and a reduced speed with a great variability of extent in cochlear outer hair cells. As demonstrated by numerical simulations, our theoretical description of mechano-electrical transduction could account for the characteristics of transduction currents in wild-type and mutant hair cells, both vestibular and cochlear. The confrontation of electrophysiological recordings and simulations led us to propose that harmonin-b operates as an intracellular link that limits the extent of adaptation and engages adaptation motors. This dual role is consistent with the scaffolding property of the protein and its binding to both actin filaments and the tip link component cadherin-23 near the tip link upper insertion point (Michalski et al., 2009). Electrophysiological recordings were performed by Nicolas Michalski during his PhD under the supervision of Christine Petit.

III. THE HAIR-BUNDLE AMPLIFIER

Spontaneous hair-bundle oscillations provide a characteristic frequency to the hair cell. I describe here how a hair cell can benefit from oscillatory force production by its hair bundle to actively resonate with weak external sinusoidal stimuli and in turn amplify its responsiveness.

1. Mechanical amplification

1.1 Power gain

By applying small sinusoidal mechanical stimuli with a flexible glass fiber (Fig. 5), the linear response function $\tilde{\chi}(\omega) = \langle \tilde{X}(\omega) \rangle / \tilde{F}(\omega)$ of a hair bundle can be measured as a function of angular frequency ω, where $\tilde{X}(\omega)$ and $\tilde{F}(\omega)$ represent the Fourier components at ω of the hair-bundle position X and of the external force F, respectively . In the case of a control hair bundle that does not oscillate spontaneously, the phase difference $\varphi(\omega) = \arg(\tilde{\chi}(\omega))$ between the response and the stimulus is always positive and increases with frequency (Fig. 13A). As expected for a passive mechanical system that is subjected to viscous friction, the movement of the hair bundle lags the external driving force. In the case of an oscillatory hair bundle, however, $\varphi(\omega)$ changes sign near the characteristic frequency of spontaneous oscillation. At low frequencies, the response displays a phase lead. Such behavior can happen only in an active system, because it indicates that the hair bundle pumps energy *into* the stimulus fiber to evoke the observed movement (Fig. 13B). In other words, the dissipative part of the response function is negative! Under such circumstances, a conservative estimate of the active work $\overline{W}_A$ produced by the hair cell during one cycle of stimulation yields $\overline{W}_A \approx +80$ zJ, corresponding to 1-2 molecules of ATP hydrolyzed per cycle of stimulation (Martin and Hudspeth, 1999). Because hair-bundle friction may be an order of magnitude larger than first anticipated (Nadrowski et al., 2004), this measurement clearly represents an underestimate. By comparing the bundle's spontaneous oscillations to its response to small mechanical stimuli (Fig. 13C), we showed (Martin et al., 2001) that an oscillatory hair bundle violates a fundamental principle of systems at thermal equilibrium, the fluctuation-dissipation theorem (Callen and Welton, 1951). A hair bundle's spontaneous movements as well as its responsiveness to sinusoidal stimuli at frequencies near that of the spontaneous oscillation are produced by energy-consuming elements within the hair cell.

The hair cell's ability to power spontaneous oscillations of its mechanosensory organelle has important functional consequences. The modulus $|\tilde{\chi}(\omega)|$ of the response function characterizes the bundle's sensitivity to external stimulation and has units of compliance (Fig. 13D). Within the range of stimulus frequencies that we explored, a control hair bundle (no oscillation) displays a low sensitivity that does not vary significantly. In contrast, the sensitivity of an oscillatory hair bundle is tuned and is about 5-fold greater than that of the

control bundle near the characteristic frequency of spontaneous oscillation. Spontaneous hair-bundle oscillations thus offer a characteristic frequency near which the hair cell actively resonates with sinusoidal stimuli and in turn amplifies its responsiveness to sinusoidal stimuli. The hair-bundle amplifier offers a double benefit for auditory detection: it enlarges the range of sound intensities that can be detected by enhancing the response to the weakest stimuli and it sharpens frequency selectivity by filtering the input to the hair cell. Note that amplification results here from phase entrainment of noisy hair bundle movements by the stimulus. As the stimulus gets more intense, the bundle's response at the stimulus frequency grows at the expense of other frequency components of bundle motion: the power produced by the hair cell to drive its hair-bundle movements is progressively funneled at the frequency of stimulation.

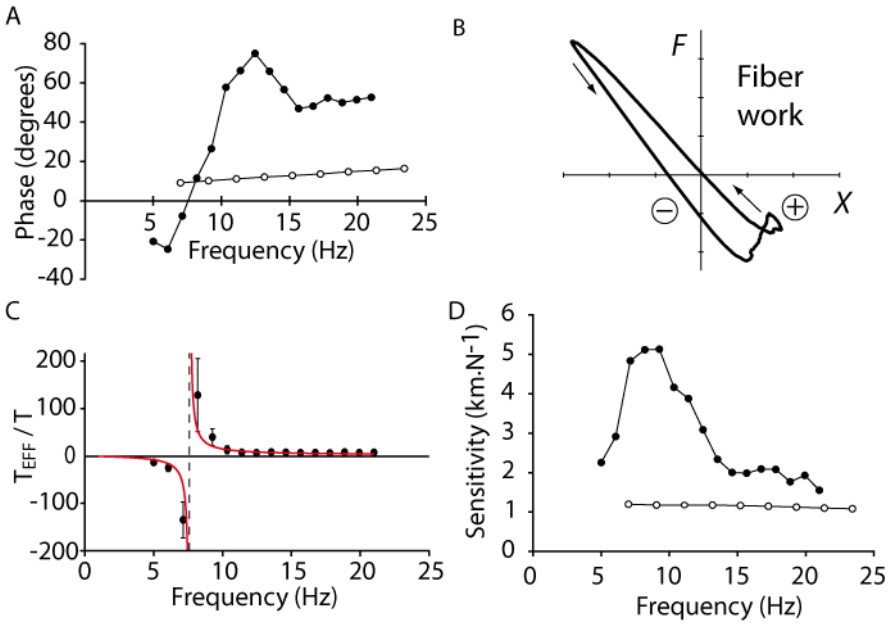

Fig. 13: Amplification by active hair-bundle oscillation. A: Phase difference between hair-bundle motion and external force at varying frequencies of sinusoidal stimulation for a hair bundle that oscillated spontaneously at 8 Hz (●) and for a control cell that did not show oscillations (○). B: The work produced by the stimulus fiber during one cycle of oscillation is measured from the area under the curve that represents the external force F (scale: 1 pN) as a function of bundle position X (scale: 10 nm). A clockwise rotation corresponds to energy delivered to the hair bundle by the fiber (+); a counterclockwise rotation indicates instead that energy is absorbed from the hair bundle by the fiber (-). Here, the net fiber work is negative; correspondingly, the hair bundle pumps +40 zJ of energy into the fiber to sustain its movement. This hair bundle was stimulated below its characteristic frequency of oscillation. C: An effective temperature T_{EFF} can be defined to relate, at each frequency of stimulation, the power spectrum of spontaneous fluctuations of position to the dissipative part of the linear response function of the hair bundle. For a system at thermal equilibrium, this effective temperature must equal room temperature T. Deviations from T quantifies violation of the fluctuation-dissipation theorem. Here, T_{EFF} diverges and changes sign at the characteristic frequency of spontaneous oscillation. D: As a result of mechanical amplification, the sensitivity of an oscillatory hair bundle (●) is enhanced by ~5-fold near the characteristic frequency of spontaneous oscillation as compared to the low sensitivity of a control non-oscillatory cell (○). The data shown in A, C and D are from the same cells. Data shown in A and D from (Martin and Hudspeth, 2001), in B from (Martin and Hudspeth, 1999) and in C from (Martin et al., 2001).

1.2 Compressive nonlinearity – Gain of the hair-bundle amplifier

When an oscillatory hair bundle is subjected to sinusoidal stimuli of increasing magnitudes, the magnitude of the response exhibits a growing behavior that depends on frequency. Stimulation at frequencies much higher than the bundle's characteristic frequency of spontaneous oscillation (stimulation "off-resonance"; see Fig. 13D) evokes a nearly linear response of low and constant sensitivity throughout the range of stimulus amplitudes (Fig. 14). In contrast, near the characteristic frequency of spontaneous oscillations ("at resonance"), the bundle's response displays a compressive nonlinearity (Fig. 14). For small stimuli, the response increases linearly but swiftly and the bundle's sensitivity correspondingly saturates at a high constant value. There the hair-bundle motion is ~5-fold larger than that measured off-resonance. For moderate to intense stimuli, the sensitivity decreases. In this regime, the dependence of response magnitude X_{RMS,ω_S} on the stimulus magnitude Δ is well described by a power law $X_{RMS,\omega_S} \propto \Delta^{1/3}$. The hair-bundle sensitivity correspondingly varies as $\Delta^{-2/3}$. Finally, for intense stimuli, the response becomes linear again and the sensitivity reaches a plateau.

This low sensitivity nearly equals that of passive cells that do not display spontaneous hair-bundle oscillations and that measured at high stimulus frequencies (off-resonance). This suggests that stimulation at intense levels or at high frequencies evokes passive responses of an oscillatory hair bundle. This inference makes intuitive sense, because the hair-bundle response, here defined as the magnitude of the Fourier component at the frequency of stimulation, should be only weakly affected by active hair-bundle movements when the stimulus is so intense that the contribution of active hair-bundle movements to the overall response becomes negligible or when the frequency mismatch between the stimulus and the active process is too large. By comparing the passive and active behaviors of the hair bundle, one can define the gain of the amplificatory process. Using the ratio of the sensitivity at resonance to small stimuli and that to intense or high-frequency stimuli, an oscillatory hair bundle from the bullfrog's saccule amplifies its phase-locked response to minute stimuli by approximately 5-fold.

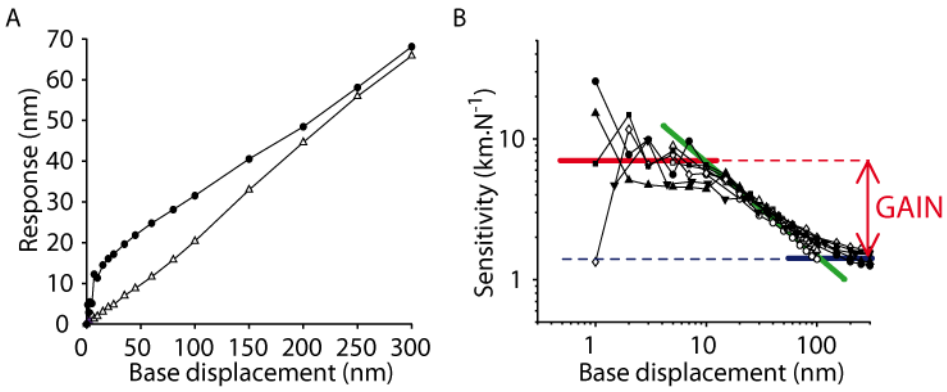

Fig. 14: Compressive nonlinearity A: Magnitude of hair-bundle movement at the frequency of stimulation as a function of stimulus intensity, here defined as the amplitude of motion imposed to the stimulus fiber's base. The response of the hair bundle is shown "at resonance" (stimulation near the characteristic frequency of spontaneous oscillations, here 9 Hz) and "off-resonance" (at 150 Hz). B: Doubly-logarithmic plot of hair-bundle sensitivity as a function of stimulus intensity for five oscillatory hair bundle stimulated at resonance. The hair bundle displays a linear regime of maximal sensitivity for small stimuli, where amplification is most effective. The sensitivity then declines to reach a low constant value that corresponds to the passive hair-bundle sensitivity that is observed off-resonance. The green oblique line depicts a power-law with a power -2/3. The ratio of maximal ("active"; red line) and minimal ("passive"; dark blue line) sensitivities defines the gain of the hair-bundle amplifier. Reproduced from (Martin and Hudspeth, 2001)

2. Two-tone distortions and suppression by the hair-bundle amplifier

Amplification by means of active hair-bundle oscillation introduces a prominent compressive nonlinearity (Fig. 14). The hair-bundle amplifier is thus expected to distort inputs with frequency components that enter the active bandwidth of the amplifier. We have recently studied the response of single oscillatory hair bundles (characteristic frequency f_C) to a force stimulus containing two sinusoidal components at nearby frequencies f_1 and f_2 ($f_2/f_1 = 1.1$) and of same intensity F. Under such circumstances, the spectral density of hair-bundle motion not only contains primaries at f_1 and f_2 but also Fourier components at linear combinations of f_1 and f_2 that are not present in the two-tone stimulus. The hair bundle thus indeed distorts its inputs.

When the hair-bundle is stimulated at resonance (Fig. 13D; f_1 and f_2 near f_C), the most prominent distortion products happen at frequencies $2f_1$-f_2 and $2f_2$-f_1 (Fig. 15A, C and E). These cubic distortions appear at low levels of stimulation ($F \sim 1$ pN), show a linear growth for weak stimuli and a compressive growth (as $\overline{F}^{1/3}$) for more intense stimuli that resemble the amplified growth of the primaries (similar to that shown in Fig. 14A). Correspondingly, the relative level of the distortion with respect to a primary (f_1 or f_2) is nearly constant at about 15% (Fig. 15E). For moderate to intense stimuli, the hair bundle produces other odd

distortions at frequencies $f_1 - k\Delta f$ and $f_2 + k\Delta f$, where k is a positive integer ($k < 5$) and $\Delta f = f_2 - f_1$. Distortion products of increasing order k are arranged according to a hierarchy that is well described by an exponential decay of their magnitude X_k: $X_{k+1}/X_k = \exp(-\lambda)$. At resonance, the coefficient λ (>0) displays strong dependences on the frequency mismatch Δf: a larger mismatch results in weaker distortions, *i.e* λ increased with Δf (not shown). These properties contrast with those observed off-resonance (f_1 and $f_2 >> f_C$; Fig. 15B, D and E). There, quadratic distortions f_1+f_2 and f_2-f_1 can instead emerge first. Cubic distortions are produced only for relatively intense stimuli ($F > 3$ pN), show a steep increase with F (as F^3) until they saturate. As expected for a passive nonlinearity, distortions are thus negligible for weak stimuli and progressively become more prominent as the stimulus becomes more intense until saturation affords no further increase of the distortion amplitude. Moreover, the intensity of the distortion products is relatively insensitive to the frequency mismatch f_2-f_1.

In addition to two-tone distortions, we also observed that the hair-bundle response to a stimulus of frequency $f_1 \cong f_C$ diminishes in the presence of a second stimulus of frequency f_2 (Fig. 15F). This nonlinear phenomenon of two-tone suppression reveals itself when the frequency mismatch between the two components of the stimulus is small enough. Much less suppression is observed with $f_1, f_2 >> f_C$.

For a given stimulus intensity, the phenomena of two-tone distortions and masking are much more pronounced at resonance, where the hair bundle amplifier enhances sensitivity to weak inputs (Fig. 13), than off resonance, for which the hair bundle works as a passive mechanical antenna. This observation makes sense because amplification introduces a prominent compressive nonlinearity for frequency components that fall within the active bandwidth of the amplifier (Fig. 14). Nonlinear two-tone interference thus appears as a natural consequence of frequency selective amplification afforded by spontaneous hair-bundle oscillations. Distortion products and two-tone suppression at the level of a single (oscillatory) hair bundle display similar properties as those evinced by phantom tones and suppressive masking in the field of psycho-acoustics (Section I.1). Because in vivo the mammalian cochlea displays active nonlinear mechanics that qualitatively resembles that of oscillatory hair bundles (Ruggero et al., 1992), this may be more than a simple coincidence. Our experimental observations suggest that active nonlinear oscillators shape the sensation of

sounds at the periphery of the vertebrate ear. This work was performed by Jérémie Barral during his PhD in my group. The data is unpublished but a manuscript will soon be submitted.

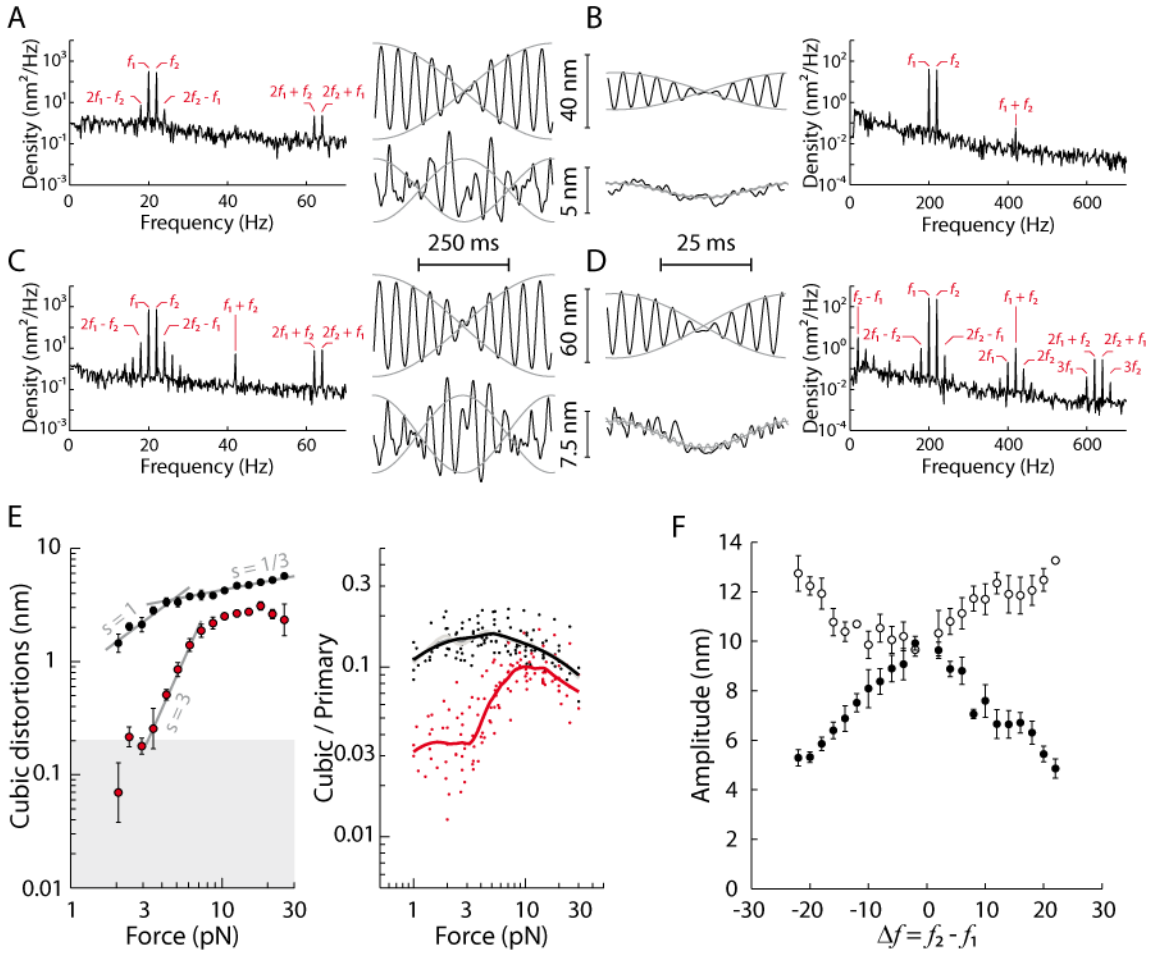

Fig. 15: Two-tone interference. A-D: Response of a hair bundle oscillating spontaneously at f_C = 20 Hz to a two-tone stimulus at resonance (A and C; f_1 = 20 Hz and f_2 = 22 Hz) or off resonance (B and D; f_1 = 200 Hz and f_2 = 220 Hz) with a magnitude F = 2 pN (A and B) or 4.8 pN (C and D). In each panel, the top temporal trace represents the full hair bundle's response; the corresponding spectral density is shown on its side. The lower temporal trace was obtained by filtering out the primaries at f_1 and f_2 from the bundle's motion; the remaining movement reveals the distortion products. E: The magnitude of the cubic distortion product $2f_2$-f_1, either absolute (left) or relative to that of the primaries (right), is plotted as a function of the external force at resonance (black disks) and off resonance (red disks). F: The magnitude of the primaries (white disks: f_1; black disks: f_2) is plotted as a function of the frequency mismatch f_2-f_1, with f_1 fixed at f_C = 22 Hz, for a two-tone stimulus of 2 pN. Unpublished data.

3. A useful concept: critical oscillation at a Hopf bifurcation

The mechanical responsiveness to sinusoidal stimuli of a single oscillatory hair bundle from the bullfrog's saccule qualitatively resembles that evinced by the mammalian cochlear partition in vivo. In both cases, the response is tuned: there exists a characteristic frequency at

which the system's sensitivity peaks (Fig. 1C and 13D). The sensitivity is maximal when it is most needed, for weak stimuli, but declines at increasing stimulus intensity before reaching a low constant level at intense stimuli (Fig. 1D and 14B). Remarkably, for moderate-to-intense stimuli, this compressive nonlinearity of sensitivity is well-described by a power law with a power of -2/3. The similar behaviors of hair-bundle and cochlear amplifiers do not necessarily imply that oscillatory hair bundles are at work in the mammalian cochlea; however, the resemblance suggests that the active process obeys the same physics in both systems. The discussion below is reproduced from a recent review that I wrote with Jim Hudspeth and Frank Jülicher (Hudspeth et al., 2010).

The key features of the active process have been recognized by theorists as signatures of a particular form of instability in dynamical systems, the Hopf bifurcation (Choe et al., 1998; Camalet et al., 2000; Eguíluz et al., 2000; Duke and Jülicher, 2008; Hudspeth et al., 2010). A Hopf bifurcation represents an oscillatory instability that occurs abruptly as a quantity C describing some component of the system—the control parameter—is varied continuously. With hair bundles from the bullfrog's saccule, the extracellular endolymphatic Ca^{2+} concentration clearly provides a control parameter of spontaneous hair-bundle oscillations (Fig. 6 and 9). A dynamical system that operates near a Hopf bifurcation is called a *critical oscillator*; it is endowed with properties that do not depend on the detailed mechanism that underlies the oscillatory behavior. The generic behavior of a critical oscillator is described by a dynamic equation, called the normal form, of a complex variable Y:

$$\frac{dY}{dt} = -\left(C - C_C - i\omega_C\right)Y - b\left|Y\right|^2 Y + \frac{F}{\Lambda}. \qquad (7)$$

If $X \equiv \mathrm{Re}(Y)$ describes the displacement of a mechanical system and F represents a stimulus force, Λ has the units of a friction coefficient. Although the response of the nonlinear system includes components at the integer harmonics of the stimulus frequency, we shall consider only the dominant terms associated with the frequency of stimulation. If the system is subjected to a sinusoidal stimulus $F = \overline{F}e^{i\omega t}$ at frequency ω, the normal form imposes a steady-state response $Y = \overline{X}e^{i\omega t}$ in which the amplitude $\overline{X}$ displays a nonlinear relation to the stimulus amplitude $\overline{F}$:

$$\overline{F} = A\overline{X} + B\left|\overline{X}\right|^2 \overline{X}. \qquad (8)$$

The linear component of the response is described by the impedance $A = \Lambda\left[\left(C - C_C\right) + i\left(\omega - \omega_C\right)\right]$ and the nonlinear term by the coefficient $B = \Lambda b$. In the limit of weak stimulation, the system displays a linear sensitivity $\chi = \left|\overline{X} / \overline{F}\right| = 1/\left|A\right|$. The sensitivity shows a resonance when the critical oscillator is stimulated at its characteristic frequency $\omega = \omega_C$ (Fig. 16A and C). The width of the resonance in the linear regime is $\Delta\omega_{lin} \cong \left|C - C_C\right|$.

At the bifurcation, $C = C_C$ and the critical oscillator displays a striking behavior that cannot occur in a passive system: if the system is stimulated at its characteristic frequency $\omega = \omega_C$, the linear coefficient A vanishes. As a consequence, the response is governed by the nonlinearity. For an increasing amplitude of stimulation, the amplitude $\overline{X}$ displays a compressive growth described by the power law $\left|\overline{X}\right| \propto \left|\overline{F}\right|^{1/3}$ (Fig. 16B). The sensitivity χ therefore varies as $1/\left|\overline{F}\right|^{2/3}$, which formally diverges for small stimuli (Fig. 16D). For a critical oscillator at resonance, there is *no* stimulus weak enough to elicit a linear response. In that sense, a critical oscillator displays an *essential* nonlinearity. In contrast, a passive system always displays linear behavior in response to weak sinusoidal stimuli: $\left|\overline{X}_{passive}\right| \propto \left|\overline{F}\right|$. This property arises because frictional forces can never disappear unless internal sources of energy can be mobilized to produce negative damping. By compensating for the frictional forces, a critical oscillator acts as an active amplifier.

We can define the gain G of the amplificatory process by comparing, for the same stimulus, the response of a critical oscillator to that of an identical system in which the active process is absent: $G = \left|\overline{X} / \overline{X}_{passive}\right| \propto 1/\left|\overline{F}\right|^{2/3}$. This relation demonstrates that the amplifier is nonlinear and preferentially boosts weak signals. In addition, the sensitivity of a critical oscillator displays nonlinear frequency tuning. When plotted against stimulus frequency at a given force amplitude (Fig. 16C), the sensitivity displays a peak centered at ω_C and of a width given by $\Delta\omega_{active} \propto \left|\overline{F}\right|^{2/3}$. Tuning thus becomes increasingly sharp at low levels of stimulation. Note that the peak width and the sensitivity are inversely related; for faint stimuli, the product $\Delta\omega_{active}\left|\overline{X}\right|/\left|\overline{F}\right|$ is constant. Weak stimuli are therefore detected at resonance both with high sensitivity and with sharp frequency selectivity.

A critical oscillator is ideally suited for the detection of sinusoidal stimuli. By amplifying preferentially weak inputs, this active system naturally displays compressive nonlinearity and provides a large dynamic range of responsiveness. Because nonlinear amplification is strongest at frequencies near the characteristic frequency of the critical oscillator, the system additionally manifests nonlinear frequency tuning. Each critical oscillator is tuned to a specific frequency, so the analysis of complex sound stimuli calls for the operation of an assembly of oscillators with distributed characteristic frequencies.

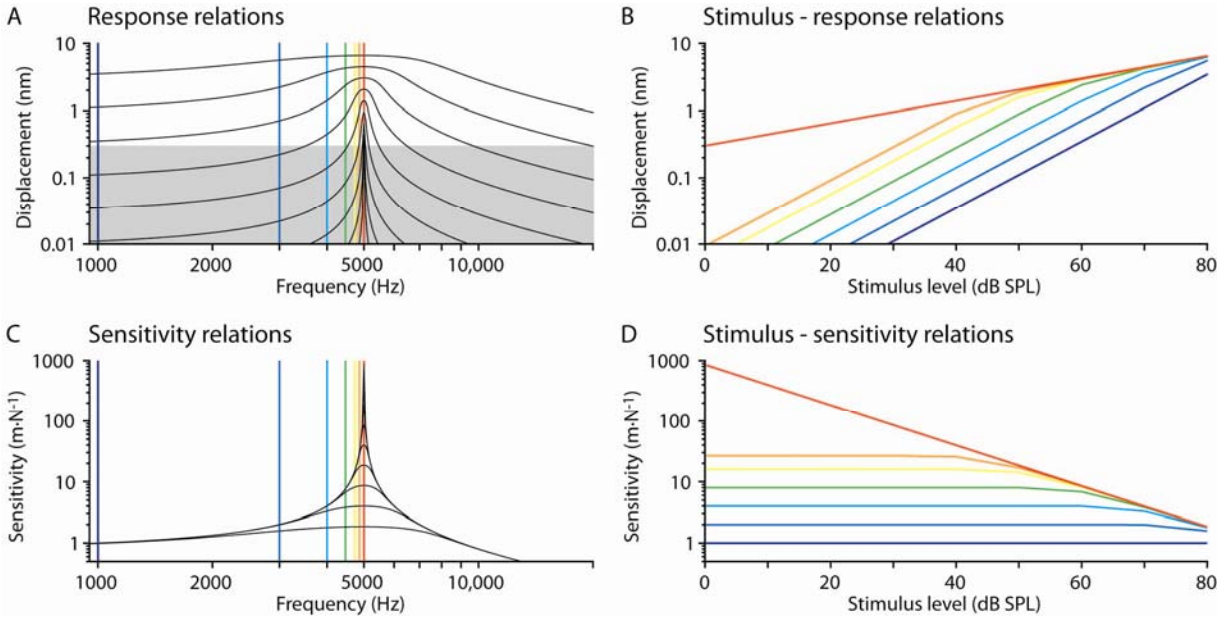

Fig. 16: Amplification by a critical oscillator. A: a doubly logarithmic plot of the magnitude of the oscillator's response as a function of stimulus frequency for a range of stimulus amplitudes. The stimuli vary in 10-dB steps from 0 dB, corresponding to the lowest curve, to 80 dB, the highest. The weakest stimuli produce significant responses only at the characteristic frequency of 5 kHz. As the stimulation becomes stronger, responses become apparent over a wider range of frequencies. The shaded area corresponds to the noise level for hair cells, about 0.3 nm; only responses larger than this elicit neural activity. B: plotting the magnitude of the response against the stimulus amplitude demonstrates the compressive nonlinearity of a critical oscillator. The 7 relations correspond to the frequencies marked by the corresponding colored lines in A. At the characteristic frequency, the relation (red) displays the slope of 1/3 characteristic of a critical oscillator. At frequencies distant from the characteristic frequency the responses are linear. C: the oscillator's sensitivity is determined by dividing its output by its input at each frequency and for each level of stimulation. The sensitivity peaks for the lowest level of stimulation and declines progressively as the forcing becomes stronger. D: at the characteristic frequency, a double-logarithmic plot of the sensitivity (red) as a function of the stimulus amplitude shows the characteristic slope of -2/3. The flat relations observed at other frequencies indicate linear responsiveness. Reproduced from (Hudspeth et al., 2010).

4. Intrinsic fluctuations and amplification by active hair-bundle oscillation

The responsiveness of an oscillatory hair bundle to sinusoidal stimuli (Fig. 14; section III.1.2) displays power-law behaviors that resemble those associated to noiseless active systems operating close to a Hopf bifurcation (Fig. 16; section III.3). However, the bundle's

sensitivity to small stimuli saturates, whereas that of a critical oscillator can be arbitrarily large. Could the sensitivity of the hair bundle be greater than has so far been observed? Hair-bundle oscillations are noisy. Intrinsic fluctuations of various origins jostle the response of a single hair bundle to weak stimuli and seriously limit amplification. We have studied theoretically the deleterious effects of noise on the hair-bundle amplifier (Nadrowski et al., 2004; Jülicher et al., 2009) and showed experimentally that an oscillatory hair bundle can overcome intrinsic noise limitations through mechanical coupling to neighbors (Barral et al., 2010).

4.1 Stochastic simulations of active hair-bundle motility

Using the physical description of active hair bundle motility that I briefly introduced in Section II.4, one can compute a state diagram of all the possible dynamical states that a hair bundle can assume in the absence of fluctuations (Nadrowski et al., 2004). Most parameters of the description are constrained by mechanical measurements, in particular by the shape of the bundle's intrinsic force-displacement relation (see for instance Fig. 7 in Section II.1.2, page 30) and by adaptation kinetics. With those parameters fixed, the state diagram is calculated as a function of only two control parameters: the Ca^{2+}-feedback strength S and the maximal force that the adaptation can produce F_{MAX} (defined in Section II.4). When the hair bundle displays a region of negative stiffness in its force-displacement relation, the diagram contains an oscillatory region at intermediate values of the control parameters (Fig. 17A). Interestingly, there is a line that delineates a border between oscillatory states and a monostable states: on this line, the dynamical system operates precisely at a Hopf bifurcation and in turn produces all the generic properties of a critical oscillator (Fig. 16).

Oscillations are noisy (Fig. 6). By destroying, the phase coherence of spontaneous oscillations, fluctuations conceal the bifurcation that may be present in a deterministic system. Fluctuations of hair-bundle position originate from at least three mechanisms. First, noise results from Brownian motion of fluid molecules that collide with the hair bundle. The fluctuation-dissipation theorem imposes that the root-mean-squared value of the corresponding fluctuating forces be proportional to the viscosity of the endolymph that bathes the hair bundle. A second source of mechanical noise is intimately related to the function of the hair bundle as a mechano-sensory antenna. Ion channels display stochastic switching

between their open and closed states: for an open probability $P_o = 0.5$, each channel spends half of its time open and the other half closed. Because mechano-to-electrical transduction channels are connected to elastic gating springs, channel clatter results in fluctuations of gating-spring (and tip-ink) tension that shake the hair bundle. In the case of an oscillatory hair bundle, we estimated that channel noise should in fact dominate noise of hydrodynamic origin (Nadrowski et al., 2004). This surprising finding can partly be explained because the condition of negative stiffness imposes large single-channel gating forces and because oscillatory hair bundles operate near $P_o = 0.5$, where gating-force fluctuations are of maximal magnitude (see Equation 2, page 31). Assuming that channels can equilibrate quickly enough to be a thermal equilibrium, the fluctuation-dissipation theorem indicate that channel clatter may be responsible for an increase of hair-bundle friction by ~10-fold from the usual hydrodynamic friction! This inference ought to be tested experimentally, for instance by measuring hair-bundle friction with and without channels blocked or as a function of the channels' open probability. Finally, a third source of (non thermal) noise arises from the stochastic binding/unbinding of the adaptation motors to the actin cytoskeleton of the stereocilia, which elicits fluctuations in the active motor force that pulls on the gating springs.

Taking these various sources of intrinsic noise into account, it was possible to produce stochastic simulations in quantitative agreement with measurements of spontaneous hair-bundle oscillations (Fig. 17B) and of linear and nonlinear response functions of the oscillatory hair bundle to sinusoidal stimuli (Nadrowski et al., 2004). By exploring all possible dynamic states that the hair bundle can endorse within its state diagram, it was shown that a hair bundle from the bullfrog's saccule operates near an optimum of frequency selectivity (Fig. 17C) and mechanosensitivity (Fig. 17D). In other words, the hair bundle cannot perform much better considering the amount of noise to which it is subjected. Fluctuations restrict the system's sensitivity to oscillatory stimuli as well as the range of stimulus magnitudes over which the compressive nonlinearity of the bundle's response occurs. This work was performed in collaboration with Frank Jülicher (MPIPKS, Dresden) and his PhD student Björn Nadrowski. The results that I summarized in this section constitute the main achievement of Björn's PhD thesis.

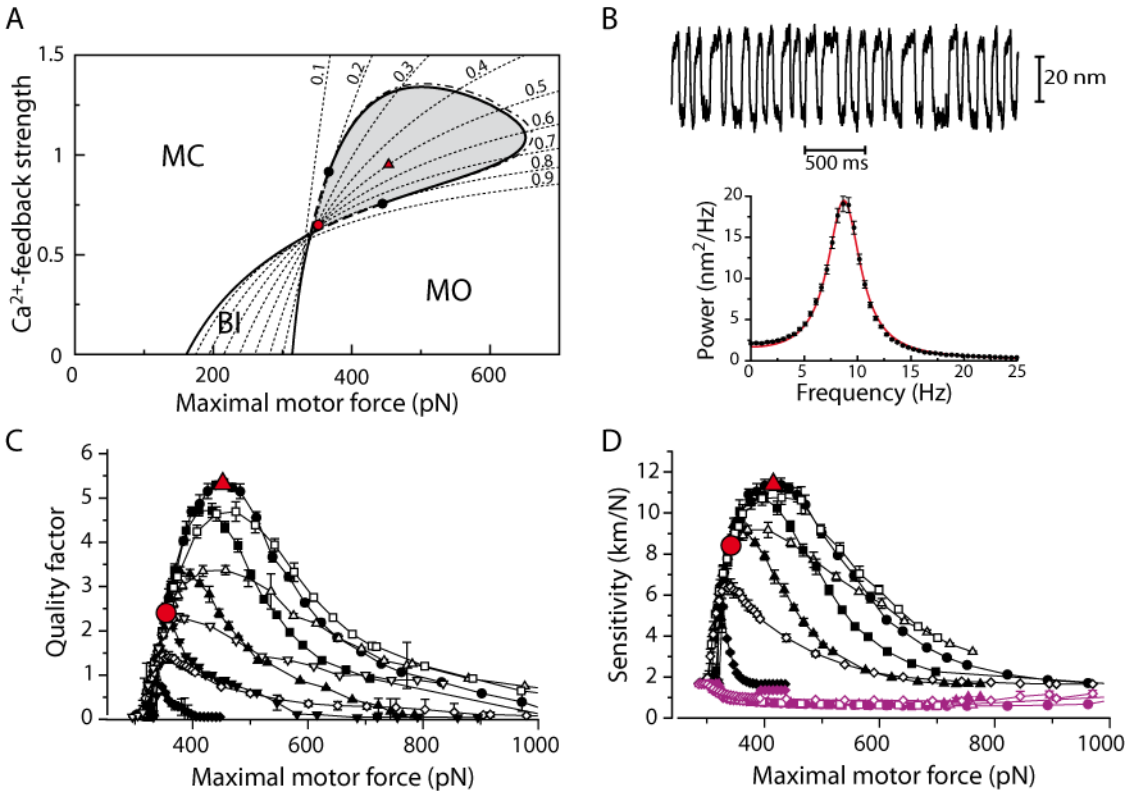

Fig. 17: A: State diagram of a deterministic description of a hair-bundle mechanics with negative stiffness. As a function of the Ca^{2+}-feedback strength (S) and the maximal force that adaptation motors can exert (f_{MAX}, here given along the tip-link axis), the hair bundle can be monostable with most channels closed (MC), monostable with most channels open (MO), bistable (BI) or oscillatory (grey region). When the operating point was set at the red disk, stochastic simulations (shown in B) reproduced the behavior of an experimentally characterized oscillatory hair bundle. The optimal operating point sits at the red triangle. B: Spontaneous oscillation and power spectral density produced by a simulation corresponding to the operating point shown by the red disk in A. C: Quality factor of spontaneous oscillation along different lines of equal open probability (shown as dotted lines in A) as a f unction of the maximal motor force. In the presence of fluctuations, oscillations are most regular near the center of the oscillatory region of the state diagram, and display a global maximum of quality (red triangle) on the line P_0 =0.5 (black disks). D: Sensitivity to weak (black) and intense (purple) sinusoidal stimuli along lines of equal open probability as a function of maximal motor force. Again, the global maximum is obtained at P_o = 0.5. The hair bundle that was experimentally studied sits near the global optimum of mechanosensitivity (red disk). Adapted from (Nadrowski et al., 2004).

4.2 Spontaneous movements and linear response of noisy oscillators: a general theoretical study

Hair cells provide a nice example to study the general properties of active mechanical oscillators. As described by Equations 3 and 4 (Section II.4, page 36), a simple deterministic model with only two degrees of freedom has been identified to explain how hair-bundle oscillations occur through a Hopf bifurcation. Proximity to a Hopf bifurcation ensures that through a sequence of analytic, but nonlinear, coordinate changes, the equations describing the dynamics of these two degrees of freedom can be condensed into a single equation, called the

normal form, of a single complex variable (Equation 7, page 48). As already noted, intrinsic fluctuations conceal the Hopf bifurcation that may be present in a deterministic system. However, by using the hair-bundle model as a reference, we showed that signatures of the bifurcation remain if noise is sufficiently weak. In particular, the linear response function obeys the same functional form as for the noiseless system on the stable side of the bifurcation but with effective, renormalized parameters. Moreover, in specific cases, we could relate analytically the bare parameters of the normal form with added noise to the bundle's effective stiffness and friction that can be estimated experimentally from the power spectrum of spontaneous activity and the linear response function to external stimuli. Importantly for hair-cell function, it was shown that the maximal sensitivity that the system can achieve in response to weak sinusoidal stimuli at the characteristic frequency of the oscillator is inversely related to noise intensity. In other cases, numerical simulations were used to determine the effects of noise and nonlinearities on effective parameters. This work was performed in collaboration with Jacques Prost (ESPCI and Laboratoire PCC, Institut Curie) and the group of Frank Jülicher (MPIPKS, Dresden), in particular Kai Dierkes and Benjamin Lindner.

4.3 Boosting the hair-bundle amplifier by mechanical coupling to "cyber clones"

As detailed in Section III.4.1, a single hair bundle is inevitably subjected to intrinsic mechanical fluctuations that restrict both the gain and the frequency selectivity afforded by spontaneous hair-bundle oscillations. In an excised preparation of the bullfrog's sacculus, the gain of a single hair-bundle amplifier, defined as the ratio of sensitivities to low versus large stimuli, saturates near a value of 5 (Fig. 14, page 45). In contrast, in vivo measurements of cochlear vibrations in mammalian preparations indicate that the gain is 100-1000 (Fig. 1, page 18). In an intact organ, however, hair bundles are most often attached to overlying membranous structures and may thus benefit from mechanical coupling to neighbors.

To assay experimentally the effects of coupling on the hair-bundle amplifier, we developed a technique of dynamic force clamp which combines mechanical stimulation of a single hair bundle from the bullfrog's sacculus and real-time simulations of oscillatory hair bundles (Barral et al., 2010). The tip of a flexible glass fiber was attached to the top of an oscillatory hair bundle and its position was measured by a photometric device at a sampling frequency of 2.5 kHz. Parameters within a stochastic physical description of hair-bundle mechanics

(Equations 3 and 4, Section II.4, page 36, with added noise terms) were adjusted to quantitatively reproduce the spontaneous movements and response to sinusoidal stimuli that were measured with the hair bundle (Nadrowski et al., 2004). We thereby produced a "cyber clone" of the experimentally observed hair bundle. For each sampled position of the hair bundle, we then calculated the intercellular forces F_1 and F_2 that this hair bundle would experience if it were flanked by two hair bundles of similar characteristics and coupled to each of them by a spring of stiffness K (Fig. 18A). The two neighboring hair bundles were here emulated by two autonomous cyber clones of the real bundle. The force $F_K = F_1 + F_2$ was applied to the hair bundle by actuating the position of the fiber's base with a piezoelectric device (Fig. 5, page27). At the same time step, the reaction forces $-F_1$ and $-F_2$ were included in the simulations of the cyber clones. The hair bundle and the cyber clones thus dynamically influenced each other's behavior.

In response to increasing coupling strength K, we observed a progressive synchronization of the hair bundle with its cyber clones (Fig. 18B)and that spontaneous hair-bundle oscillations became more regular: coupling resulted in effective noise reduction (Fig. 18C). By adding an external sinusoidal force F_{EXT}, we measured the sensitivity of the hair bundle to faint stimuli at frequencies near that of the spontaneous oscillation. We found that sensitivity increased by up to twofold with increasing coupling strength (Fig. 18D-E). These observations are in close agreement with theoretical predictions (Dierkes et al., 2008). Our results demonstrate that mechanical coupling of noisy oscillatory hair bundles can enhance amplification by a single oscillator. This property might explain the extraordinary gain of amplification that is achieved in vivo in an intact hearing organ. Simulations indeed indicate that an oscillatory module that would recruit a few tens of hair cells would be sufficient to account for the properties of cochlear amplification in mammals. This work is the result of a close collaboration with the group of Frank Jülicher (MPIPKS, Dresden). Experiments were performed jointly by Jérémie Barral (PhD student in our group) and Kai Dierkes (visiting PhD student from the group of Frank Jülicher).

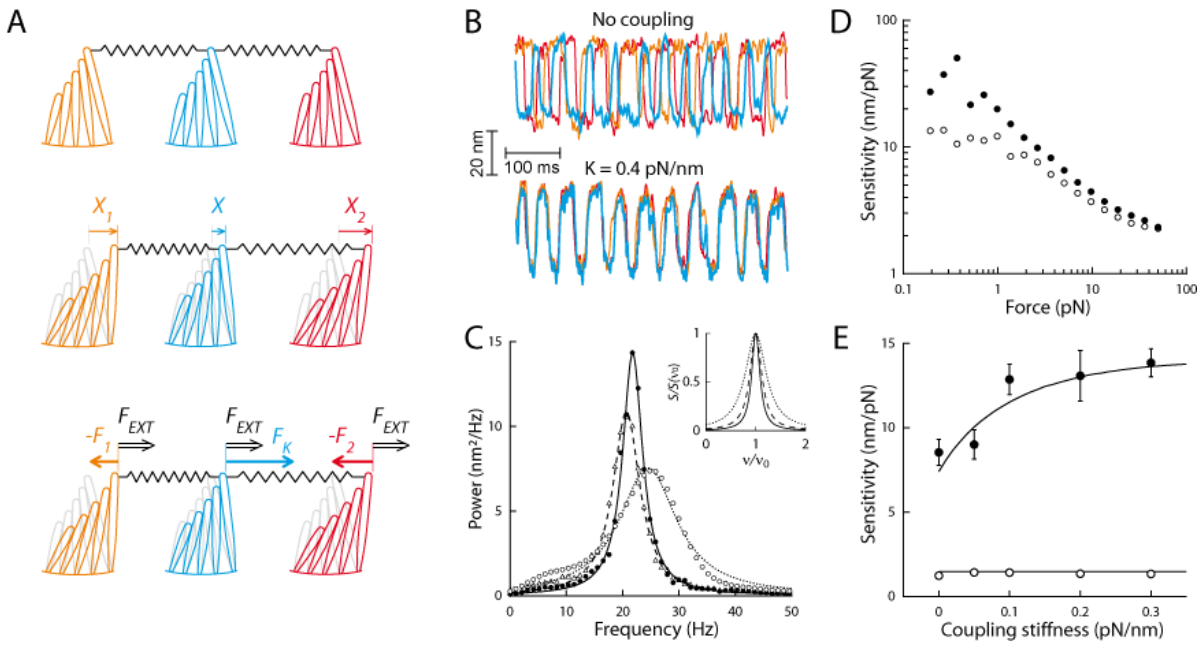

Fig. 18: Effects of coupling on the hair-bundle amplifier. A: Schematic representation of the coupled system. A hair bundle (blue) is connected to one neighbor on each side (orange and red) by identical springs of stiffness K. The positions of the hair bundles (X_1, X and X_2) oscillate spontaneously. Relative movements of adjacent hair bundles yield elastic intercellular forces ($-F_1$, F_K and $-F_2$). All three hair bundles experience the same external force F_{EXT}. The force F_K was calculated in real time from a stochastic computer simulation which emulated the behavior of the two neighbors, called cyber clones. B: Spontaneous oscillations of a hair bundle (blue) and of its cyber clones (orange and red) without coupling (top) and with coupling stiffness K = 0.4 pN/nm (bottom). C: Power spectral densities of hair-bundle movement for K = 0, 0.2, 0.4 pN/nm (dotted, broken and continuous lines, respectively). The spectra were fitted by Lorentzian functions. Inset: Spectra S normalized by their respective peak value $S(\nu_0)$ as a function of normalized frequencies ν/ν_0. D: Hair-bundle sensitivity as a function of the external force F_{EXT} without coupling (white disks) and with a coupling stiffness K = 0.2 pN/nm (black disks). E: Hair-bundle sensitivity at F_{EXT} = 0.5 pN (black disks) and F_{EXT} = 50 pN (white disks) as a function of coupling stiffness. Simulations yielded similar sensitivities shown by thin lines. Reproduced from (Barral et al., 2010).

IV. ACTIVE MOTILITY OF A MINIMAL ACTO-MYOSIN SYSTEM IN VITRO

The hair-cell bundle of the vertebrate ear offers one example of a biological system that can mobilize internal resources of biochemical origin to power mechanical oscillations. Spontaneous oscillations are in fact observed in a large variety of active systems. Insect fibrillar flight muscles, for instance develop oscillatory tension with a rhythm that is asynchronous to activating nervous impulses. Skinned skeletal and cardiac muscle fibers also exhibit spontaneous oscillations in vitro under various conditions of partial activation, for the latter even in the absence of proteins that normally regulate contractility of the muscle. Spontaneous oscillations have also been observed in nonmuscular motor systems, such as the mitotic spindle during asymmetric cell division, or some insects' antennal hearing organs. In all these cases, oscillations rely on the collective activity of molecular motors that work

against an elastic load. At the end of 2004, I decided to diversify my research by developing a simple biomimetic acto-myosin system to study the dynamical mechanical properties of small motor assemblies in vitro.

The experimental work that I summarize below was performed by Pierre-Yves Plaçais (PhD student; PhD thesis defended in June 2008) and, in its early developments by Martial Balland (former postdoc, now Maître de Conférence at the University of Grenoble, France). We benefited from a collaboration with the group of Jean-François Joanny in our department; Thomas Guérin, a PhD student in this group, performed the stochastic simulations.

1. Collective motor oscillations

To test the ability of a motor assembly to oscillate spontaneously, we have modified a conventional "gliding assay" (Fig. 19). In this experiment, a single actin filament is attached to a micron-sized silica bead and brought in contact with a myosin-coated surface by micro-manipulating the bead with optical tweezers (Plaçais et al., 2009). The bead serves both as a handle to hold the filament and as a reporter of the position of the filament end to which it is bound. When actin interacts with myosin, the (static) optical trap exerts an elastic restoring force that opposes active force production on the actin filament by the motors. Note that this simple system retains only the two essential proteins of muscle contraction, actin and myosin, and mimics the functional unit of the muscle (the half-sarcomere) but that there is no "transduction channel" or Ca^{2+} feedback. Our original goal was to work in collaboration with the group of Christine Petit (Institut Pasteur) on unconventional myosin-1c, the putative motor of the hair-bundle amplifier. Despite several attempts, however, baculovirus infection of Sf9 insect cells resulted in the production of only a very little amount of protein which in addition showed no sign of life in motility assays. We thus used instead conventional Heavy-Mero Myosins (myosin 2). This protein was readily available in the Laboratoire PCC because it had earlier been given (by mistake!) to Giovanni Cappello by Mathias Rief (TUM, Münich). I am indebted to Mathias for his kind permission to use this protein, which was directly purified from rabbit pectoral muscle in his group.

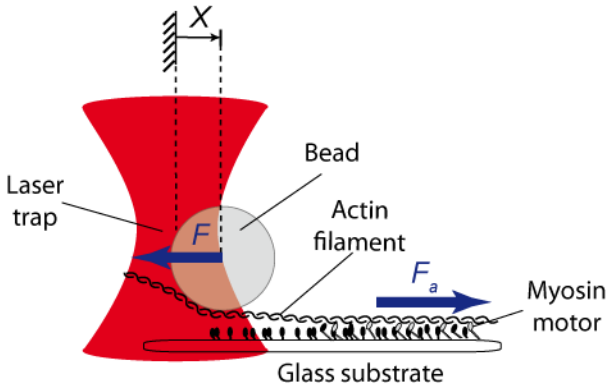

Fig. 19: A: Gliding assay with elastic loading. The motor molecules develop an active force F_a on the actin filament in a direction defined here as positive. The optical trap imposes an elastic restoring force $F = -k_T X$ in the negative direction. k_T represents the trap stiffness and X the position of the bead with respect to the center of the trap.

In the presence of ATP, the myosin assembly that interacts with the actin filament developed an active force of ~3.5-27.5 pN that was on averaged balanced by an equal and opposite elastic restoring force exerted by the tweezers. Assuming that each myosin molecule develops a force of 1.5 pN and spends 14% of its ATPase cycle bound to actin, this stall force indicates that each filament recruited a pool of 15-130 motor molecules among which 2-18 interacted with the filament at any given time. A striking characteristic of our recordings was the frequent occurrence of noisy spontaneous oscillations (Fig. 20) with peak-to-peak amplitudes within a range of 9-87 nm. Rhythmic activity was characterized by the presence of a clear peak in the spectral density of bead motion that was centered at a nonzero frequency ν_0 = 1.5-14 Hz, which defined the characteristic frequency of the oscillation. The movement waveform could resemble the asymmetric triangular oscillations that are observed in muscle or the more rectangular pattern of hair-bundle oscillations. Using stochastic simulations (Plaçais et al., 2009), we showed that our findings accord quantitatively with a general theoretical framework (Jülicher and Prost, 1997) where oscillatory instabilities emerge generically from the collective dynamics of molecular motors under load. The theory indicate that a motor assembly can actively produce a force that amounts to negative friction; if negative motor friction overcomes passives sources of positive friction the system can become self oscillatory.

Because our motor system is minimal, any complex machinery comprising assemblies of myosin-2 motors under load is expected to display the same generic properties. Our observations may thus be relevant for describing mechanical oscillations in a large variety of muscular systems. However, our in vitro system does not suffice to account for spontaneous oscillations of the hair-cell bundle in the vertebrate ear (Section II.1). Indeed, although the

mechano-to-electrical apparatus comprises assemblies of molecular motors that actively exert tension on elastic gating-springs (Fig. 2, page 21), spontaneous hair-bundle oscillations rely on electro-mechanical feedback by the Ca^{2+} component of the transduction current (Fig. 6, page 35). In particular, oscillations stop upon iontopheretic application of a channel blocker (Fig. 6B).

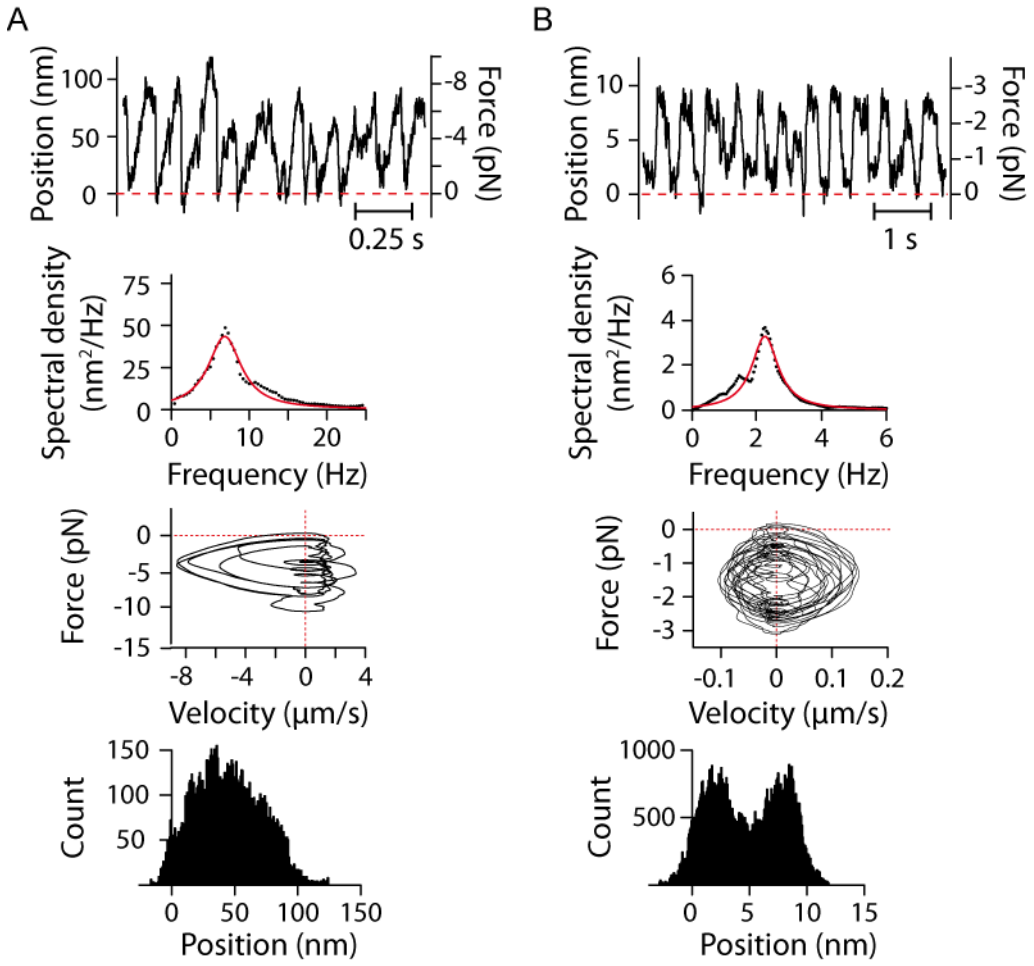

Fig. 20: Spontaneous oscillations. A and B from top to bottom bead position (with corresponding trap forces) as a function of time, spectral densities (smoothed and fitted with a Lorentzian function), relations between trap force and bead velocity, and position histograms. Data reproduced from (Plaçais et al., 2009)

2. Dynamical responsiveness of a motor collection to mechanical stimuli

During the PhD of Pierre-Yves Plaçais, we have developed an experimental setup to study the dynamic mechanical response of the acto-myosin system to external stimuli (Fig. 21). This set-up combines optical tweezers, acousto-optic deflectors to stir the laser beam, fluorescence microscopy and photorelease of molecules that can regulate the mechanical

activity of myosin. In particular, using digital feedback to control the position of the bead and a command signal of triangular waveform, we can measure the force that must be applied to the acto-myosin system to clamp the bead velocity at a constant value.

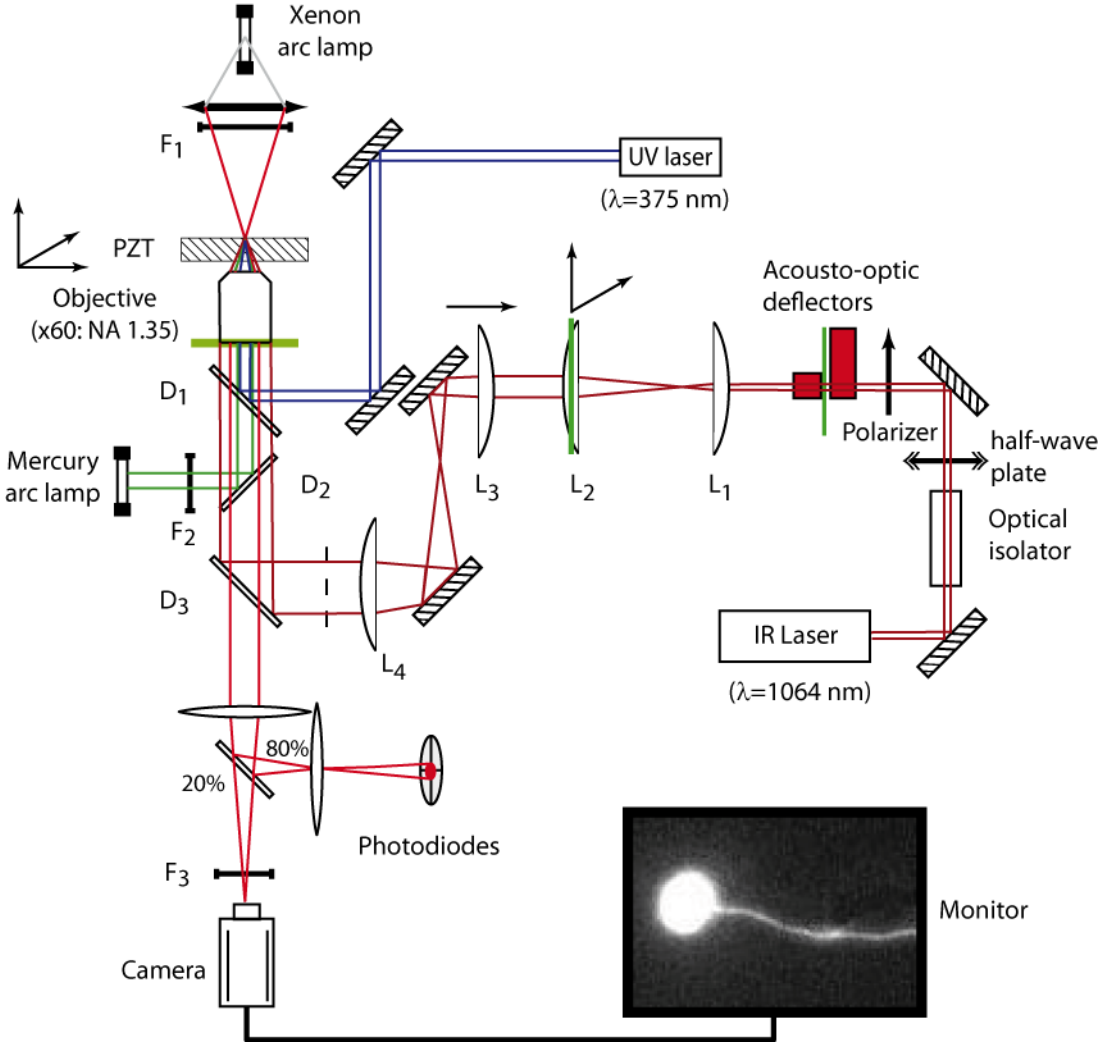

Fig. 21: Experimental set-up for the study of collective motor mechanics. <u>*Optical trap:*</u> *the infra-rayed beam from a Nd-YAG laser (Spectra Physics) emitting continuously at 1064 nm with a 4W maximal output power is directed through an optical isolator, a half wave plate and a polarizer, successively, before being diffracted by a dual-axis acousto-optical deflector (AOD) driven by a digital frequency synthetizer. The first-order diffracted beam is then magnified ×10 by two successive telescopes (L_1-L_2 and L_3-L_4), enters the microscope through a lateral camera port and is redirected by a dichroic mirror (D_3) to the back aperture of the microscope objective (X60; 1.35 numerical aperture). The AODs allows fast movement of the optical trap in the focal plane of the objective.* <u>*Displacement monitor:*</u> *Bead position is measured along two perpendicular axis in the focal plane of the objective by a displacement monitor that includes a four-quadrant photodiode onto which an image of the bead is projected at a magnification of ×625 using the brightfield illumination of a Xenon arc lamp filtered by a long-pass cutoff filter (F_1).* <u>*Fluorescence visualization:*</u> *Light from a mercury arc lamp passes through the excitation filter (F_2). Light emitted by the fluorophore is filtered by an emission filter (F_3) that is positioned before the camera. An example of a single bead-tailed actin filament is shown on the monitor.* <u>*Uncaging*</u>*: A continuous UV laser emitting at 375 nm enters the microscope just below the objective and is re-directed to the objective's back-focal plane by a dichroïc mirror (D_1).*

In the presence of ATP, the force exerted by the optical trap in response to a velocity-clamp protocol can display a behavior that depends on the directionality of bead movement (Fig. 22A and B). For forward bead movements, corresponding to motion in the direction that the motors would impose if no load were present and defined here as positive (Fig. 19), the time course of the force is well fitted by an exponential rise that can be extrapolated to a steady-state force $F_V(V>0)$. As would be expected for a "regular" motor system, the trap force F_V that opposes active motor forces has to be decreased in magnitude to increase the velocity of forward bead motion (Fig. 22C). Stall force is nearly identical to that measured when the displacement-clamp feedback loop is disengaged. When no external force is applied ($F_V = 0$), the bead velocity is similar to those measured in standard gliding assays. In contrast to positive movements, bead movements in the negative direction elicit a behavior that resembles that observed in the absence of ATP: a force jump at the ramp onset is followed by an approximately linear variation of the force with time. The stiffness associated with the elastic component of the response does not depend on velocity and its value $k_L = 0.079 \pm 0.07$ pN·nm^{-1} is close to those measured with no ATP. Subtracting this elastic contribution to the total force measured in response to negative bead velocities yields a force which, at a given velocity, quickly reaches a steady state level $F_V(V<0)$. A prominent feature of the relation between the force F_V and velocity is that it displays a region of negative slope at velocities between -5 μm·s^{-1} and -1 μm·s^{-1} (Fig. 22C). Within this interval, faster backward motion of the bead results from smaller backward pulling forces by the optical trap, a remarkable behavior which amounts to negative friction. Non-monotonic relations between trap force F_V and velocity were observed only in the presence of ATP.

These promising unpublished observations were obtained in only three experiments. They need to be repeated in a more controlled environment, in particular to avoid non-specific interactions between the bead and the substrate. Such interactions indeed often produced parasitic elastic components in the force that was measured, eventually causing the bead to stick to the glass substrate and thus limiting the success rate of the experiment. Although the elastic force component that is apparent in Figure 22B at negative bead velocities must be considered with caution, it is hard to imagine that such parasitic stiffness would cause the non-monotonic behavior that is shown in Figure 22C.

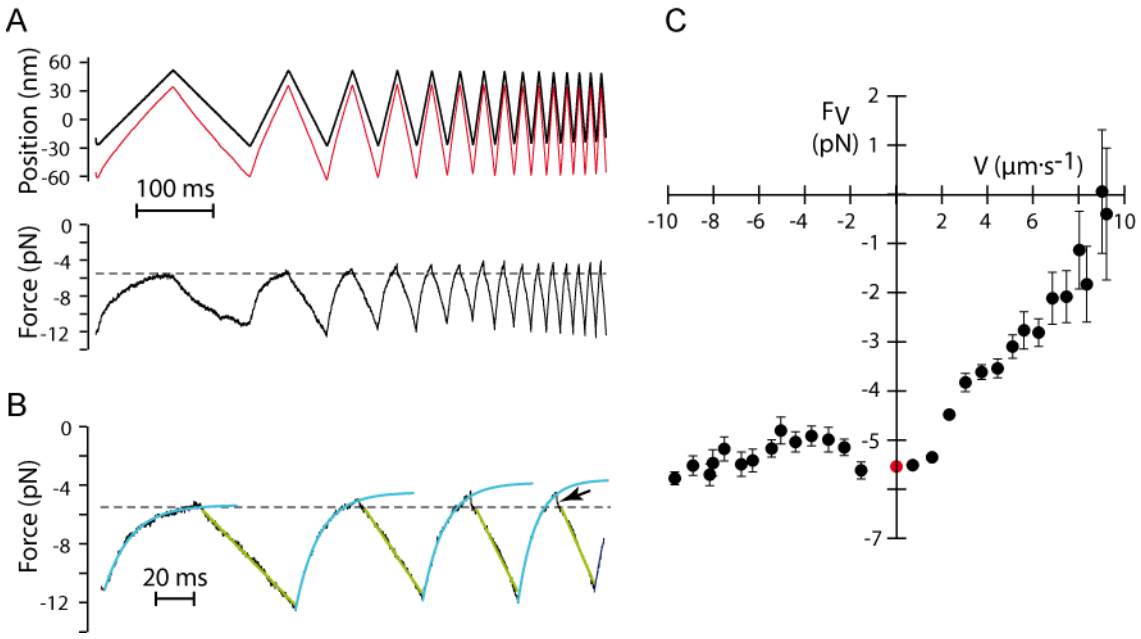

Fig. 22: A: Top: position of the bead (black) and of the optical trap (red) as a function of time. During each ramp, the bead moved at constant velocity. Bottom: the corresponding force exerted on the bead by the optical trap. Stall force is indicated by an horizontal broken line. B: Enlargement of the beginning of the record shown in A for the force. In the positive direction (= direction of motor-force production), the time-course of the force could be fitted by an exponential (light blue line) from which we estimated, for each ramp, the asymptotic force F_V that the system would have reached if the ramp lasted longer. In the negative direction, a fast jump at the initiation of each ramp (arrow) was followed by a nearly linear increase of the force (green line), indicating the presence of an elastic element. The magnitude F_V of the frictional component of the force was estimated by substrating the elastic response. C: Plot of the force F_V as a function of bead velocity. The relation displys an anomalous region of negative slope. Unpublished data.

C. FUTURE DIRECTIONS

I. Active hair-bundle motility by mammalian hair cells

Vertebrate hearing relies on nonlinear amplification of sound inputs to achieve exquisite sensitivity, and sharp frequency selectivity, and to operate over a dynamic range that can span six orders of magnitude of sound-pressure level. Our past research promotes a general principle of auditory amplification that is based on the generic physical properties of "critical" mechanical oscillators, *i.e.* of active dynamical systems that operate near an oscillatory instability called a Hopf bifurcation. Using the bulfrog's sacculus as a model system, we showed that the hair cell can power noisy oscillations of its mechano-sensory hair bundle at 5-150 Hz, a frequency range that falls within the sensitivity range of this low-frequency organ. Active hair-bundle motility is the only candidate for the auditory amplifier in non-mammalian vertebrates. In mammals, active hair-bundle motility coexists with somatic electromotility, by which the "piezoelectric" soma of outer hair cells in the cochlea changes its length in response to changes of the cells' transmembrane potential. Electromotility has been shown to be necessary for cochlear amplification. However, electrical filtering of receptor potentials by the membrane capacitance of the outer hair cell as well as the lack of frequency selectivity of this form of motility raise serious doubts about the ability of this process to operate on its own. Although active hair-bundle movements have been measured in the rat cochlea in response to force steps (Kennedy et al., 2005), no spontaneous oscillations have yet been observed in mammals. Worse, mechanical oscillations beyond a few hundred hertz have yet to be directly observed in a biological system and it remains to be demonstrated that molecular motors, which are thought to underlie active motility in frog, can drive oscillations at auditory frequencies. In this respect, note that we also plan to address the issue of fast periodic force production by a motor assembly by using minimal acto-myosin molecular systems in vitro; see below. Although there is ample in vivo evidence that the mammalian cochlea indeed powers mechanical oscillation at frequencies up to a few tens of kilohertz, the cellular and molecular processes that underlie high-frequency motility remains a central question of auditory physiology.

To tackle this question at the cellular level, it appears necessary to develop an in vitro preparation of the mammalian cochlea. As starters, we may adapt cochlear preparations that have already been developed by our collaborators, either of the gerbil (with Jim Hudspeth, the Rockefeller University, New York) or of the rat (with Christine Petit, Institut Pasteur, Paris). Because most of the attention has so far been devoted to electromotility alone, a systematic study of hair-bundle mechanics is still lacking in a mammalian system. Key to the success of the approach, we will reproduce the two-ionic compartments that hair cells experience in vivo: although the soma of these epithelial cells are immersed in a conventional perilymphatic fluid that is rich in sodium ions, the hair bundles are bathed in a potassium-rich and calcium-poor endolymph. We know from past experience in frog that the Ca^{2+} concentration in endolymph controls active hair-bundle motility (see Sections B.II.1 and B.II.3). In particular, no spontaneous oscillations can be observed if this concentration is outside a certain range. In addition, we will impose a voltage difference of +100 mV between the endolymphatic and perilymphatic compartments to mimic the endocochlear potential that magnifies the magnitude of transduction currents, including their Ca^{2+} component. Under these conditions, we will test the ability of mammalian hair bundles to produce active movements, in particular spontaneous oscillations. We will also measure force-displacement relations and response functions to sinusoidal stimuli along the tonotopic axis of the organ, from low-frequency to high-frequency hair cells. Unlike the bullfrog's sacculus, which does not present any tonotopic organization of its hair cells, the mammalian cochlea makes it possible to test how (active) hair-bundle mechanics vary with the characteristic frequency of the hair cell and in turn helps define frequency selectivity. For hair cells with characteristic frequencies beyond a few kilohertz, it will probably be necessary to develop mechanical actuators with faster rise times (<100 μs) than those provided by flexible glass fibers (>300 μs).

II. Fluctuation-Response relation with an oscillatory hair-cell bundle

The fluctuation-dissipation theorem is a central result of statistical physics that relates, for any system at thermal equilibrium, linear response function and fluctuations. We have shown in the past that hair cells showing spontaneous oscillations of their mechanosensitive hair bundle violate the fluctuation-dissipation theorem. We took this result as evidence that hair-

bundle movements result from an energy-consuming mechanism that drives the system out of equilibrium. As any active dynamical system that operates in the vicinity of a Hopf bifurcation, hair-bundle dynamics can be characterized by a frequency-dependent effective temperature that diverges at the characteristic frequency of spontaneous oscillation (Fig. 13C; page 43). Recently, Jacques Prost and colleagues have shown that for any system with Markovian dynamics, even in a non-equilibrium steady state and with non-energy-conserving dynamics, a proper choice of observables restores a relation between fluctuations and response (Prost et al., 2009).

We wish to use the hair-cell bundle to test the applicability of this new theorem to an active mechanical system. Spontaneous hair-bundle oscillations are simply described by a dynamic interplay between only two "slow" variables (Tinevez et al., 2007): the hair-bundle position X and the position X_a of the molecular motors that set tip links under tension (see Fig. 1D in Results section). Of these two relevant variables, only the hair-bundle position can be measured directly. The transduction current I that flows into the hair cell through open transduction channels, however, can also be measured with a patch-clamp technique. Because I is a (nonlinear) function of X-X_a, the observables (X, I) should be sufficient to describe active hair-bundle dynamics. We will measure the fluctuations of these variables and their response to external forces. In collaboration with Jacques Prost and Jean-François Joanny, we will then compute a new set of variables that should satisfy a generalized fluctuation-dissipation theorem.

III. Dynamic mechanical properties of molecular-motor assemblies

Using a minimal motile system comprising only a bead-tailed actin filament and a few tens of myosin molecules, we have recently demonstrated that a motor assembly can produce spontaneous oscillations under load (Section B.IV.1). The mechanism responsible for the oscillatory behavior as well as the parameters that define frequency and amplitude of oscillation, however, remain to be extensively characterized experimentally. We have already developed an experimental procedure to measure the force that the bead-tailed actin filament must undergo to move at constant velocity (Fig. 22; Section B.IV.2). Our preliminary experiments, however, suffered from non-specific interactions between the bead and the substrate. In addition to testing various passivating treatments, we plan to take advantage of

microfabricated pedestals to keep the bead away from any surface while the actin is interacting with the motors.

In collaboration with the team of Cécile Sykes in our department, we have also started performing gliding assays with bundles composed of a few tens of cross-linked actin filaments (using fascin and/or formin in conjunction with profilin). These actin bundles are expected to recruit a larger number of myosin molecules than the single filaments that we previously used, possibly resulting in more regular and long-lasting oscillations under load. In addition, being much more rigid than single filaments, actin bundles should allow better external control of the oscillation frequency with the load's stiffness. In our previous assays (Plaçais, 2008), we had indeed observed that the entropic stiffness of a single actin filament was often significantly lower than that of the optical trap; the oscillation was in turn relatively insensitive to a change in trap stiffness.

Finally, we plan to extend our experiments on myosin 2 (Heavy Mero-Myosin from rabbit pectoral muscle) to other myosin types, in particular those implicated in the hair-bundle oscillator of hair cells. With hair cells from the saccule of the bullfrog, the most likely motor to mediate hair-bundle oscillations is myosin 1c, a single-headed myosin with slow ATPase kinetics. The team led by Evelyne Coudrier (UMR144, Institut Curie) can produce a very similar motor, myosin 1b. The group of Cécile Sykes in our department has also recently provided myosin-1c molecules that were given by her collaborator Michael Ostap (University of Pennsylvania, Philadelphia). We have already successfully performed gliding assays with myosin 1b but not, so far, with myosin 1c. These two unconventional myosins produce their power stroke in two steps, a property that is associated with strong sensitivity to external forces (Laakso et al., 2008): the rate of myosin-1b detachment from actin decreases by more than 75-fold when under tension of 2 pN or less! Contrary to other motors, like kinesin, that tend to detach more often under load, this motor stays attached and sustains the additional tension created by an opposing external force. We will determine in our in vitro assay whether, as one would intuitively (and perhaps naively) anticipate, this condition stabilizes the motor assembly. On the other hand, some steps in the ATPase cycle of myosin-1c have been shown to be regulated by calcium, resulting in an acceleration of detachment and a lengthening of the lifetime of the myosin detached state at increased Ca^{2+} concentrations (Adamek et al., 2008). In hair cells, forward motion of the motors increases tension in the tip

links, in turn evoking a larger Ca^{2+} influx through transduction channels and an increase of the Ca^{2+} concentration at the motor site (Fig. 1D, page 21). In accordance with the aforementioned biochemical evidence, hair-bundle mechanics suggests that calcium weakens the motors (Fig. 4), possibly through its interaction with the calmodulin molecules that are attached to the myosin neck of myosin 1c. Effectively, Ca^{2+} feedback fosters load-dependent detachment of the motors: a stimulus-evoked increase in gating-spring tension - the external force that pulls on the motor - evokes a Ca^{2+} influx that favors motor detachment. This property may potentially lead to a dynamical instability through a cooperative attachment-detachment of the motor collection (Howard, 2009; Guerin et al., 2010). Using feedback and Ca^{2+} uncaging, we will mimic Ca^{2+} changes associated with motor motion in hair cells by increasing the local Ca^{2+} concentration near the motors when we measure a bead movement in the direction of the motor force. The system may go into spontaneous oscillation as the result of Ca^{2+} interactions with myosin. The effects of Ca^{2+} on motor-force production may also be studied at the single molecule level using a "three-bead assay", a technique that we have developed earlier in the team during the PhD of Pierre-Yves Plaçais.

We will characterize the dynamic mechanical properties of the acto-myosin assembly by applying three types of stimuli. First, we will repeat preliminary experiments by imposing ramp displacements to the bead to estimate the force-velocity relation of the system at steady state. We aim at confirming that spontaneous motor oscillations are associated with a region of negative slope in the force-velocity relation and, in collaboration with the theorists led by Jean-François Joanny in our department, correlate the amplitude, waveform and frequency of the oscillation with the shape of the force-velocity relation. Second, we will apply step displacements of various magnitudes to the bead and measure the force that is developed by the motor system over time. In the absence of (parasitic) elastic elements between the actin and the glass substrate, the system is endowed with translational invariance; the force that is measured should thus relax to zero. Similar motor movements are thought to underlie "adaptation" of mechano-electrical transduction to step defections of the hair bundle in hair cells (see Fig 3 in Section B). By characterizing motor kinetics, our experiment may thus help determine whether the behavior of a motor assembly can account for the complex adaptation kinetics, with fast (~1 ms) and slow (~10 ms) components, that is observed in hair cells. Moreover, we will measure the force-displacement relation of the acto-myosin system at

various times after the stimulus is applied, in the presence and absence of ATP. If the system displays a non-monotonic force-*velocity* relation, it may be the case that its force-*displacement* relation contains a region of negative stiffness that is analogous to that measured with hair-cell bundles. Finally, we will measure the frequency-dependent response function of the system by applying sinusoidal displacements to the trap position. In the case where spontaneous motor oscillations are produced, we expect to observe frequency-selective, nonlinear amplification. An important challenge for the long term is to determine whether a system of molecular motors can drive spontaneous oscillations and frequency-selective amplification of weak stimuli at auditory frequencies. In this respect, the effect of the stiffness of the external load and, in the case of myosin 1b or c, on electro-mechanical feedback by Ca^{2+} ions should of interest.

This project was initiated during the PhD of Pierre-Yves Plaçais (2004-2008) and is now carried on by Jonathan Lee-Tin-Wah, a new PhD student with a background in Biology who joined the team in October 2009. Volker Bormuth, a physicist with expertise on molecular motors and optical motors has also joined the team in October 2010. Later this year, this project will form the basis of a grant proposal to the Agence Nationale de la Recherche (ANR) together with the groups of Cécile Sykes (Institut Curie, Paris) and Laurent Blanchoin (CEA, Grenoble).

REFERENCES:

Adamek N, Coluccio LM, Geeves MA (2008) Calcium sensitivity of the cross-bridge cycle of Myo1c, the adaptation motor in the inner ear. Proc Natl Acad Sci U S A 105:5710-5715.

Barral J, Dierkes K, Lindner B, Jülicher F, Martin P (2010) Coupling a sensory hair-cell bundle to cyber clones enhances nonlinear amplification. Proc Natl Acad Sci USA 107:8079-8084.

Beurg M, Fettiplace R, Nam JH, Ricci AJ (2009) Localization of inner hair cell mechanotransducer channels using high-speed calcium imaging. Nat Neurosci 12:553-558.

Callen HB, Welton TA (1951) Irreversibility and generalized noise. Phys Rev 83:34-40.

Camalet S, Duke T, Jülicher F, Prost J (2000) Auditory sensitivity provided by self-tuned critical oscillations of hair cells. Proc Natl Acad Sci USA 97:3183-3188.

Choe Y, Magnasco MO, Hudspeth AJ (1998) A model for amplification of hair-bundle motion by cyclical binding of Ca^{2+} to mechanoelectrical-transduction channels. Proc Natl Acad Sci USA 95:15321-15326.

Clausznitzer D, Lindner B, Julicher F, Martin P (2008) Two-state approach to stochastic hair bundle dynamics. Phys Rev E Stat Nonlin Soft Matter Phys 77:041901.

Duke T, Jülicher F (2008) Critical oscillators as active elements in hearing. In: Active processes and otoacoustic emissions (Manley GA, Popper AN, Fay RR, eds), pp 63-92. New York: Springer.

Eatock RA (2000) Adaptation in hair cells. Annu Rev Neurosci 23:285-314.

Eguíluz VM, Ospeck M, Choe Y, Hudspeth AJ, Magnasco MO (2000) Essential nonlinearities in hearing. Phys Rev Lett 84:5232-5235.

Géléoc GS, Lennan GW, Richardson GP, Kros CJ (1997) A quantitative comparison of mechanoelectrical transduction in vestibular and auditory hair cells of neonatal mice. Proc R Soc Lond B 264:611-621.

Gillespie PG, Gillespie SK, Mercer JA, Shah K, Shokat KM (1999) Engineering of the myosin-ibeta nucleotide-binding pocket to create selective sensitivity to N(6)-modified ADP analogs. J Biol Chem 274:31373-31381.

Goldstein JL (1967) Auditory nonlinearity. J Acoust Soc Am 41:676-689.

Guerin T, Prost J, Martin P, Joanny JF (2010) Coordination and collective properties of molecular motors: theory. Curr Opin Cell Biol 22:14-20.

Holt JR, Gillespie SK, Provance DW, Shah K, Shokat KM, Corey DP, Mercer JA, Gillespie PG (2002) A chemical-genetic strategy implicates myosin-1c in adaptation by hair cells. Cell 108:371-381.

Howard J (2009) Mechanical signaling in networks of motor and cytoskeletal proteins. Annu Rev Biophys 38:217-234.

Howard J, Hudspeth AJ (1987) Mechanical relaxation of the hair bundle mediates adaptation in mechanoelectrical transduction by the bullfrog's saccular hair cell. Proc Natl Acad Sci USA 84:3064-3068.

Howard J, Hudspeth AJ (1988) Compliance of the hair bundle associated with gating of mechanoelectrical transduction channels in the bullfrog's saccular hair cell. Neuron 1:189-199.

Hudspeth AJ, Gillespie PG (1994) Pulling springs to tune transduction: adaptation by hair cells. Neuron 12:1-9.

Hudspeth AJ, Julicher F, Martin P (2010) A critique of the critical cochlea: Hopf-a bifurcation-is better than none. J Neurophysiol in press.

Jaramillo F, Hudspeth AJ (1993) Displacement-clamp measurement of the forces exerted by gating springs in the hair bundle. Proc Natl Acad Sci U S A 90:1330-1334.

Jülicher F, Prost J (1997) Spontaneous oscillations of collective molecular motors. Phys Rev Lett 78:4510-4513.

Jülicher F, Dierkes K, Lindner B, Prost J, Martin P (2009) Spontaneous movements and linear response of a noisy oscillator. Eur Phys J E 29:449-460.

Kennedy HJ, Crawford AC, Fettiplace R (2005) Force generation by mammalian hair bundles supports a role in cochlear amplification. Nature 433:880-883.

Kossl M, Vater M (1985) Evoked acoustic emissions and cochlear microphonics in the mustache bat, Pteronotus parnellii. Hear Res 19:157-170.

Laakso JM, Lewis JH, Shuman H, Ostap EM (2008) Myosin I can act as a molecular force sensor. Science 321:133-136.

Manley GA (1990) Peripheral hearing mechanisms in reptiles and birds. Berlin Heidelberg: Springer-Verlag.

Manley GA (2001) Evidence for an active process and a cochlear amplifier in nonmammals. J Neurophysiol 86:541-549.

Martin P, Brochard-Wyart F (1998) Dewetting at soft interfaces. Phys Rev Lett 80:3296.

Martin P, Hudspeth AJ (1999) Active hair-bundle movements can amplify a hair cell's response to oscillatory mechanical stimuli. Proc Natl Acad Sci USA 96:14306-14311.

Martin P, Hudspeth AJ (2001) Compressive nonlinearity in the hair bundle's active response to mechanical stimulation. Proc Natl Acad Sci USA 98:14386-14391.

Martin P, Mehta AD, Hudspeth AJ (2000) Negative hair-bundle stiffness betrays a mechanism for mechanical amplification by the hair cell. Proc Natl Acad Sci USA 97:12026-12031.

Martin P, Hudspeth AJ, Jülicher F (2001) Comparison of a hair bundle's spontaneous oscillations with its response to mechanical stimulation reveals the underlying active process. Proc Natl Acad Sci USA 98:14380-14385.

Martin P, Bozovic D, Choe Y, Hudspeth AJ (2003) Spontaneous oscillation by hair bundles of the bullfrog's sacculus. J Neurosci 23:4533-4548.

Michalski N, Michel V, Caberlotto E, Lefevre GM, van Aken AF, Tinevez JY, Bizard E, Houbron C, Weil D, Hardelin JP, Richardson GP, Kros CJ, Martin P, Petit C (2009) Harmonin-b, an actin-binding scaffold protein, is involved in the adaptation of mechanoelectrical transduction by sensory hair cells. Pflugers Arch 459:115-130.

Moore BCJ (2004) An introduction to the psychology of hearing: Elsevier.

Nadrowski B, Martin P, Jülicher F (2004) Active hair-bundle motility harnesses noise to operate near an optimum of mechanosensitivity. Proc Natl Acad Sci USA 101:12195-12200.

Plaçais PY (2008) Propriétés mécaniques de la myosine II in vitro: de la molécule unique aux effets collectifs. In, p 207. Paris: Université Pierre et Marie Curie.

Plaçais PY, Balland M, Guérin T, Joanny JF, Martin P (2009) Spontaneous oscillations of a minimal acto-myosin system under elastic loading. Phys Rev Lett 103:158102.

Prost J, Joanny JF, Parrondo JM (2009) Generalized fluctuation-dissipation theorem for steady-state systems. Phys Rev Lett 103:090601.

Ricci AJ, Crawford AC, Fettiplace R (2000) Active hair bundle motion linked to fast transducer adaptation in auditory hair cells. J Neurosci 20:7131-7142.

Robbles L, Ruggero MA (2001) Mechanics of the mammalian cochlea. Physiol Rev 81:1305-1352.

Ruggero MA, Robles L, Rich NC (1992) Two-tone suppression in the basilar membrane of the cochlea: mechanical basis of auditory-nerve rate suppression. J Neurophysiol 68:1087-1099.

Ruggero MA, Rich NC, Recio A, Narayan SS, Robles L (1997) Basilar-membrane responses to tones at the base of the chinchilla cochlea. J Acoust Soc Am 101:2151-2163.

Russell IJ, Kossl M, Richardson GP (1992) Nonlinear mechanical responses of mouse cochlear hair bundles. Proc R Soc Lond B 250:217-227.

Shera CA (2007) Laser amplification with a twist: traveling-wave propagation and gain functions from throughout the cochlea. J Acoust Soc Am 122:2738-2758.

Stauffer EA, Scarborough JD, Hirono M, Miller ED, Shah K, Mercer JA, Holt JR, Gillespie PG (2005) Fast adaptation in vestibular hair cells requires Myosin-1c activity. Neuron 47:541-553.

Tinevez JY, Jülicher F, Martin P (2007) Unifying the various incarnations of active hair-bundle motility by the vertebrate hair cell. Biophys J 93:4053-4067.